Quaternary International 643 (2023) 46–60

Contents lists available at ScienceDirect

Quaternary International

journal homepage: www.elsevier.com/locate/quaint

Late glacial and Holocene climate in the Kunlun Pass region (northern Tibetan Plateau) inferred from a multi-proxy lake record

Wanyi Zhang [a,*], Steffen Mischke [b], Dominic Hosner [c], Chengjun Zhang [a], Birgit Plessen [d], Huwei Li [a], Xiaojing Zhang [a]

[a] School of Earth Sciences & Key Laboratory of Mineral Resources in Western China (Gansu Province), Lanzhou University, Lanzhou, Gansu, 730000, China
[b] Institute of Earth Sciences, University of Iceland, 102 Reykjavík, Iceland
[c] Eurasia Department and Beijing Branch Office, German Archaeological Institute, Im Dol 2-6, 14195, Berlin, Germany
[d] Helmholtz-Zentrum Potsdam, Deutsches GeoForschungsZentrum GFZ, Telegrafenberg C 327, 14473, Potsdam, Germany

ARTICLE INFO

Keywords:
Central Asia
Summer monsoon
Granulometry
Geochemistry
Ostracoda

ABSTRACT

Holocene environmental and climate change on the Tibetan Plateau is intensively studied and discussed with the aim to better understand the factors controlling the hydrology of individual river catchments and especially the availability of water which is of utmost significance for the communities downstream in times of rapid climate change. Thus, a late glacial and Holocene sediment record from Lake Heihai in the Kunlun-Pass region was investigated using ostracod and geochemical analyses. Cold and dry conditions were inferred between *ca.* 12.9 and 12.3 cal ka BP and higher temperatures before and afterwards. The cold spell probably corresponds to the Younger Dryas (YD) event in the North Atlantic region. Warmer and wetter conditions with highest lake levels and decreased lake-water salinity were recorded from *ca.* 10.8 to 7.0 cal ka BP when the summer monsoon was strengthened. The cold 8.2 cal ka BP event is not significantly recorded in the region probably due to the predominance of the summer monsoon over the westerlies. A declined lake level and increased lake-water salinity as the result of cold and dry conditions are inferred from *ca.* 7.0 to 4.5 cal ka BP when the strengthening of the mid-latitude westerly circulation probably triggered glacier advances in the catchment. An even lower lake level existed during cold conditions with glacier advances from *ca.* 4.5 to 1.2 cal ka BP. The level of Lake Heihai rose again after *ca.* 1.2 cal ka BP due to warmer conditions, causing the retreat of glaciers and higher runoff. Our record from the Kunlun Pass region provides further evidence for the catchment-specific response of hydrographical systems which are partly controlled by glaciers as major water sources.

1. Introduction

The hydrology and landscape of the Tibetan Plateau responses sensitively to global climate warming (Liu et al., 2021). As a result, many studies addressed past environmental and climate change in different regions of the plateau (Chen et al., 2020; Sun and Feng, 2022). Local climate conditions during the late glacial and the Holocene are typically deduced from studies of lake-sediment cores or exposed lake-sediment sections, or shoreline deposits (Lister et al., 1991; Peng, 1997; Zhu et al., 2002, 2004, 2008; Mischke et al., 2005; Shen et al., 2005; Holmes et al., 2007). Records from Qinghai Lake, Donggi Cona, Koucha Lake, Kuhai Lake, Gahai Lake, Nam Co, Pumoyum Co and other lakes provide valuable information with respect to the lake evolution during the Holocene and local environmental and climate conditions in the different catchments (Lister et al., 1991; Liu et al., 2007; Mischke et al., 2008, 2010b; Zhu et al., 2010; Li et al., 2012; Peng et al., 2013). Some of these records allowed the assessment of specific lake-external processes such as the generation and accumulation of aeolian deposits or the glacier dynamics in the lake catchments (Qiang et al., 2006; Xiao et al., 2008, 2015; Mischke et al., 2010c; Stauch et al., 2017; Wang et al., 2021). The geomorphological evolution of drainage basins is studied to reveal the response of mountain-basin systems to paleoclimate fluctuations (An et al., 2018a, 2018b). For example, periods of aggradation and incision were important geomorphological controls for the dynamic evolution of landforms in the Golmud River catchment (An et al., 2018b).

Ostracods, as bivalved micro-crustaceans, inhabit almost all types of water bodies. They have good potential as palaeoenvironmental

* Corresponding author.
E-mail address: zhangwanyi@lzu.edu.cn (W. Zhang).

https://doi.org/10.1016/j.quaint.2022.10.013
Received 26 April 2022; Received in revised form 10 October 2022; Accepted 19 October 2022
Available online 11 November 2022

indicators due to their low-magnesium calcite shell which is often well preserved in lake sediments (De Deckker et al., 1988). Species assemblages and the abundance of specimens sensitively trace changes in environmental factors, such as water depth, water temperature, specific conductivity (SC, as a measure of salinity), type of hydrophytes and substrate properties (De Deckker, 1981; Cyr and Downing, 1988; Mourguiart and Carbonel, 1994; Holmes et al., 1998; Meisch, 2000; Hirokazu, 2003; Mischke et al., 2005). Fossil shells are used for palaeoclimate inferences based on applications of an indicator-species approach, of transfer functions or the mutual climatic range method (Mischke et al., 2007, 2008, 2010c; Frenzel et al., 2010). Stable isotopes and trace elements of the calcitic shells are used to infer past conditions of water bodies such as salinity or temperature (Mischke et al., 2008, 2010b). A number of lakes on the Tibetan Plateau such as the lakes Qinghai, Donggi Cona, Koucha, Kuhai, Gahai, Nam Co and Pumoyum Co were investigated combining ostracod data with other multi-proxy data (Lister et al., 1991; Liu et al., 2007; Mischke et al., 2008, 2010b; Zhu et al., 2010; Li et al., 2012; Peng et al., 2013). These records provide valuable information about the regional evolution of lakes and related environmental variations in response to Holocene climate change.

However, accumulated evidence shows that the Holocene climate dynamics on the Tibetan Plateau were spatially heterogeneous due to the complex interactions of different moisture-transporting wind systems in the region (the westerlies, the Indian and East Asian summer monsoons) and different catchment-specific characteristics (alignment of mountain ranges with respect to prevailing winds, presence and size of glaciers, the thermokarst development and degradation, etc.; Li, 1989; Shen and Tang, 1996; Mischke et al., 2008; Ramisch et al., 2016; Stauch et al., 2017; Zhang et al., 2021).

Thus, we conducted a multi-proxy study of a late glacial and Holocene sediment core from Lake Heihai in the Kunlun Pass region. We investigated the ostracod species distribution, the ostracod-based transfer function for specific conductivity, stable oxygen and carbon isotopes of ostracod shells and bulk sediment samples, granulometry of the sediments, the total organic matter content and the carbonate content in order (1) to quantitatively and qualitatively reconstruct the lake evolution and environmental fluctuations including glacier variations in the catchment, (2) to deduce impacts of the summer monsoon and climate change in the northern part of the Tibetan Plateau.

2. Regional settings

Lake Heihai (35°57′ - 36°02′ N, 93°12′ - 93°18′ E; Figs. 1 and 2), also named Xiwangmu Yaochi, is located in an intermontane basin between the Kunlun tectonic belt and the Burhan Buda Mountains on the Tibetan Plateau with a lake elevation of 4431 m above sea level (a.s.l.). The Kunlun Mountain range lies in the south, including glaciated peaks up to 5769 m a.s.l. high. The surface area of Lake Heihai is approximately 38.7 km^2 with a NW-SE length of 10.2 km, average SW-NE width of 3.8 km and a catchment of 730 km^2. The Kunlun Fault in the south of the lake catchment is a large strike-slip fault which triggered major earthquakes (Van Der Woerd et al., 2002; Li et al., 2005). However, its influence on lake-level changes of Lake Heihai was apparently insignificant during the Holocene (Stauch et al., 2017; An et al., 2018a). In contrast, river terraces in the region formed in response to Holocene climate changes (Chang et al., 2017; An et al., 2018a, 2018b).

The catchment area in the south of Lake Heihai is dominated by Permian to Triassic slates and schists with limestones, and Oligocene to Miocene sandstones and conglomerates in smaller areas. The southeastern part of the catchment is occupied by Jurassic granites. Palaeozoic mafic rocks and Ordovician to Silurian sandstones and conglomerates occur in the northern part of the lake. The lower catchment regions are composed of unconsolidated Quaternary sediments (Kidd et al., 1988).

The lake is drained by the outflow of the Kunlun River in its southeast, which then feeds into the Golmud River in the Qaidam Basin (Wang and Dou, 1998). Permafrost features are widely distributed in the catchment area (Stauch et al., 2017; Zhang et al., 2021). Lake terraces

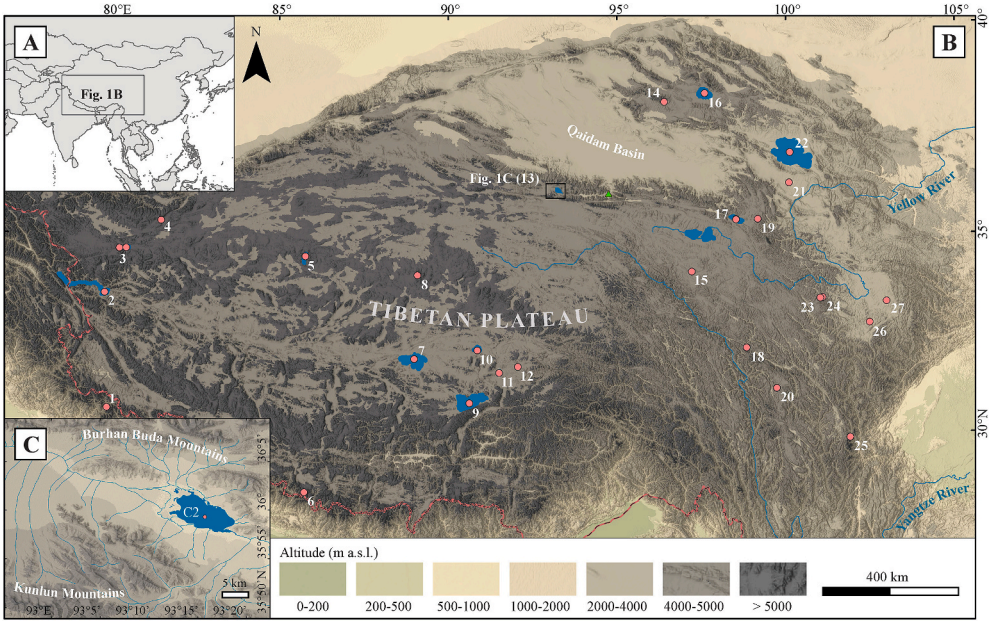

Fig. 1. The Tibetan Plateau, the location of Lake Heihai and sites with Holocene records referred to in the text. A) Location of the Tibetan Plateau, B) the Tibetan Plateau with the locations of Lake Heihai (13), other palaeoclimate studies (circles), and the Kunlun Pass (triangle); palaeoclimate studies: 1 - Dunagiri Valley (Sati et al., 2014), 2 - Bangong Co Lake (Gasse et al., 1996), 3 - Sumxi Co and Longmu Co lakes (Fontes et al., 1993), 4 - Guliya Ice Core $\delta^{18}O$ record (Thompson et al., 1997; Yao, 1999), 5 - Buruo Co Lake (Xu et al., 2019), 6 - Dasuopu Ice Core (Thompson et al., 2006), 7 - Seling Co Lake (Gu et al., 1993), 8 - Puruogangri Ice Core (Thompson et al., 2006), 9 - Nam Co Lake (Zhu et al., 2008), 10 - Zigetang Lake (Herzschuh et al., 2006), 11 - Cuoe Lake (Wu et al., 2006), 12 - Ahung Co Lake (Morrill et al., 2006), 13 - Lake Heihai (this study), 14 - Dunde Ice Core $\delta^{18}O$ and pollen records (Liu et al., 1998), 15 - Koucha Lake (Mischke et al., 2008), 16 - Hala Lake (Yan and Wünnemann, 2014), 17 - Donggi Cona Lake (Mischke et al., 2010b), 18 - Yingpu Valley (Ou et al., 2014), 19 - Kuhai Lake (Mischke et al., 2010c), 20 - Naleng Lake (Kramer et al., 2010), 21 - Genggahai Lake (Song, 2012), 22 - Qinghai Lake (Shen et al., 2005), 23 - Nianbaoyeze peat bog (Schlütz and Lehmkuhl, 2009), 24 - Ximencuo Lake (Zhang and Mischke, 2009; Herzschuh et al., 2014), 25 - Hailuogou catchment (Xu et al., 2016), 26 - Hongyuan peat bog (Hong et al., 2003), 27 - Zoige peat record (Zhao et al., 2011). C) Catchment topography of Lake Heihai and position of core C2. Administrative areas are based on GADM, version 2.8, November 2015; Elevation based on Shuttle Radar Topography Mission (SRTM) V4.1 data (Jarvis et al., 2008).

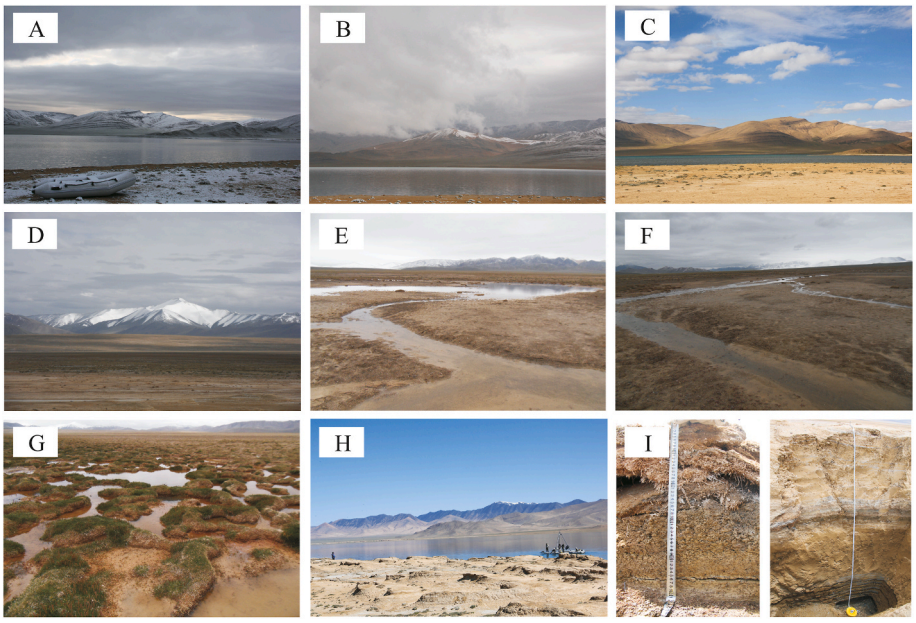

Fig. 2. Field photographs of Lake Heihai in July 2011. A-C, views of the northern side of the lake. D, view of mountain front at the southern side of the lake. E and F, streams flowing to the lake from the southeast and southwest, respectively. G, shallow swamps in the west of the lake. H, view of the lake from the southern shore. I, sections of lake terraces on the southern side of the lake.

are distributed on the western, northern and southern shores of the lake (Fig. 2, I). Shallow swamps are present on the western margin (Fig. 2, G). Alluvial fans dominate the lower regions of Lake Heihai's catchment. Two large alluvial fans in the west and southeast of the lake originate from the partly glaciated main Kunlun Mountain range (Fig. 2E and F). In the north of the lake, alluvial fans are covered by aeolian sand deposits (Stauch et al., 2017).

The climate in the region is cold and arid. The mean annual precipitation is approximately 360 mm (Maussion et al., 2014), while the annual potential evaporation is significantly higher with approximately 900 mm. The mean January temperature at the Wudaoliang meteorological station (4780 m a.s.l.) *ca.* 50 km south of Lake Heihai is −16.2 °C, and the mean July temperature is 6.2 °C (WorldClimate: http://www.worldclimate.com/). The mean annual temperature is approximately −8.0 °C (Maussion et al., 2014).

The arid climate system and high elevation of the study area are also reflected by the vegetation, with alpine steppe dominated by *Stipa purpurea* and *Carex moorcroftii* (Zhang, 2007). Lake Heihai is regarded as pristine lake due to its remoteness and low human impact by grazing and tourism. Thus, the evolution of the lake system is mainly controlled by natural climate conditions.

3. Materials and methods

3.1. General information on the investigated sediments

A sediment core C2 with a length of 670 cm was drilled at 22 m water depth in 2011, using an UWITEC platform and a modified Livingstone piston coring device. The sediments are light grey clayey silt from 670 to 610 cm, greyish silty sand from 610 to 570 cm, dark grey clayey silt from 570 to 185 cm, and laminated light greyish clayey silt from 185 to 0 cm.

3.2. Age-depth relationship and bulk sediment analysis

Lockot et al. (2015) worked on the chronology of the core and they determined a large lake-reservoir effect of 6455 ± 15 ^{14}C yr for aquatic

Table 1
Radiocarbon dates from Lake Heihai (Lockot et al., 2015).

Lab Number	Depth (cm)	Material	Species	^{14}C ka BP	Cal ka BP	Core	Reference
Poz-54598	13	Plant	*Potamogeton*	5.60 ± 35	6.37	C2	Lockot et al. (2015)
Poz-54596	68	Plant	*Potamogeton*	6.22 ± 40	7.12	C2	Lockot et al. (2015)
Poz-54605	91	Plant	*Potamogeton*	6.76 ± 40	7.62	C2	Lockot et al. (2015)
Poz-54597	113	Plant	*Potamogeton*	6.33 ± 70	7.26	C2	Lockot et al. (2015)
Poz-55272	134	Plant	*Potamogeton*	7.18 ± 50	8.00	PG	Lockot et al. (2015)
Poz-49726	177	Plant	*Potamogeton*	6.31 ± 70	7.24	PG	Lockot et al. (2015)
Poz-49727	227	Plant	*Potamogeton*	6.56 ± 40	7.47	PG	Lockot et al. (2015)
Poz-55024	237	Plant	*Potamogeton*	7.21 ± 60	8.03	PG	Lockot et al. (2015)
Poz-54599	240	Plant	*Potamogeton*	6.67 ± 40	7.54	C2	Lockot et al. (2015)
Poz-49728	266	Plant	*Potamogeton*	8.43 ± 50	9.46	PG	Lockot et al. (2015)
Poz-55025	325	Plant	*Potamogeton*	9.07 ± 80	10.24	PG	Lockot et al. (2015)
Poz-54600	362	Plant	*Potamogeton*	9.98 ± 50	11.44	C2	Lockot et al. (2015)
Poz-54604	413	Plant	*Potamogeton*	16.18 ± 120	19.53	C2	Lockot et al. (2015)
Poz-55026	468	Plant	*Potamogeton*	13.31 ± 90	16.01	PG	Lockot et al. (2015)
Poz-54601	489	Plant	*Potamogeton*	15.55 ± 80	18.81	C2	Lockot et al. (2015)
Poz-49729	490	Plant	*Potamogeton*	17.51 ± 100	21.16	PG	Lockot et al. (2015)
Poz-55027	564	Plant	*Potamogeton*	10.22 ± 60	11.93	PG	Lockot et al. (2015)
Poz-49718	565	Plant	*Potamogeton*	10.52 ± 60	12.48	PG	Lockot et al. (2015)
Poz-54602	637	Plant	*Potamogeton*	14.22 ± 100	17.31	C2	Lockot et al. (2015)

plants (*Potamogeton*) from the modern lake. The age-depth relationship was established using core C2 and a parallel shorter core PG containing several inverse ^{14}C ages (Table 1), especially below a core depth of 365 cm. They concluded that the lake-reservoir effect must have changed significantly through time and observed a correlation between the inverse ages and the input of allochthonous dolomite suggesting an impact of ^{14}C-dead carbon from a limestone catchment. They established four possible age-depth models (Fig. 3) based on the AMS ^{14}C dates (Table 1) for core sediments and estimated sediment-accumulation rates, verified by magnetic inclination and declination data. From the combined age limits of the four models, an age frame for the calibrated and reservoir-corrected ages could be derived, which shows an increasing uncertainty with increasing depth. In subsequent studies by Ramisch et al. (2016, 2018), models 3 and 4, the maximum age estimation, were selected as the most convincing solution given that first inferences were compliant with the YD chronology (Walker et al., 2008, 2012; Cheng et al., 2020). However, they limited their application to millennial scale analysis due to the existing uncertainties of the age-depth models.

Based on the occurrence of a distinct sand layer between 610 and 572 cm core depth and its assignment to the widely identified YD period, age-depth model 3 of Lockot et al. (2015) was also adopted here by applying the sediment accumulation rates provided by Lockot et al. (2015) in their Table 2 (shown as apparently erroneously named model 4 in their Fig. 5, see Fig. 3 in this study). In contrast, we did not follow the more recently suggested age-depth model of Zhang et al. (2021) who did not include lake-reservoir-effect based corrections of the original ^{14}C data and who defined the YD-Holocene boundary at 440 cm core depth based on changes of organic matter and carbonate contents which we consider insignificant at this specific stratigraphic level.

Total organic matter content (TOC) was determined by the anti-titration method with dense sulfuric acid (H_2SO_4) and potassium dichromate ($K_2Cr_2O_7$; Bao, 1999).

The carbonate content in sediments was analyzed by the gas volumetric determination “Scheibler method” (Tatzber et al., 2007). The carbonate content was measured in a carbonate analyzer device by reacting sediments with 1N hydrochloric acid (HCl) and measuring the pressure of the produced CO_2. Afterwards, the results were calculated as volume data and then converted into carbonate contents. Errors are lower than ±1%.

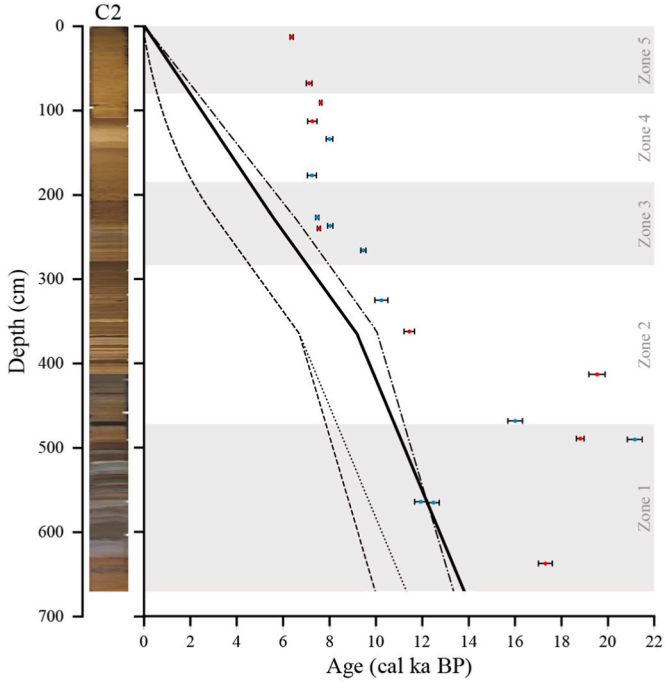

Fig. 3. Lithology for core C2 and age-depth models 1–4 for Lake Heihai (Lockot et al., 2015). The thicker, solid line indicates model 3 used in this study. Error bars represent the calibrated ^{14}C ages (Table 1), red for core C2 and blue for core PG (data from Lockot et al., 2015). (For interpretation of the references to colour in this figure legend, the reader is referred to the Web version of this article.)

Grain-size analyses were performed using a laser diffraction particle sizer Mastersizer 2000 on 266 samples at a spacing of 2 or 3 cm, after removal of carbonate and organic compounds by 10% HCl and 10% H_2O_2 treatment, respectively. To avoid coagulation, sodium pyrophosphate ($Na_4P_2O_7$ * $10H_2O$) was added, and the samples were then shaken for several hours. Before measurements, every sample was divided into eight subsamples and dispersed in an ultrasonic bath. At least three subsamples were measured in each case and their grain-size distribution was averaged.

The major mineral species of bulk sediment samples were identified by X-ray diffraction (XRD) analysis (PW2403 X, Netherlands) at the Key Laboratory of Western China’s Environmental System (Ministry of Education), Lanzhou University. Powdered sample aliquots were scanned from 10° to 70° using Cu-Kα radiation (*ca*. 0.154 nm) with pipe voltage at 40 kV and electricity at 60 mA. The scan step was 0.017°, and time between steps was 0.12 s. The semi-quantitative percentage concentration of minerals was calculated by the ratio of the peak area of a single mineral to that of all minerals. A scanning electron microscope (SEM; Zeiss MERLIN Compact FE-SEM) was used to produce images of sediment samples from the core at the Key Laboratory of Petroleum Resource Research, Northwest Institute of Eco-Environment and Resources, Chinese Academy of Sciences. Sediment samples were glued on an aluminum stub and coated with carbon.

We identified abundant authigenic carbonate in the lake sediments with a SEM. Thus, stable isotope data of bulk carbonate from Lake Heihai mainly reflect authigenic carbonate from the lake. The predominantly authigenic origin of carbonate in different lakes in western China was similarly demonstrated by Zhang et al. (2013). The formed carbonate type in these lakes is controlled by the water chemistry. Higher carbonate contents are typically produced during warmer conditions when precipitation is higher, resulting also in higher lake levels. Magnesian calcite, dolomite and aragonite gradually form with increasing salinity. The carbon and oxygen isotope composition of carbonates in lake sediments was proven as good indicator of lake water chemistry, lake depth and residence time (Zhang et al., 2013a). The comparable trends of the carbon and oxygen isotopic compositions of bulk-sediment samples and ostracod shells in zones 2 to 5 show that the stable isotope data for bulk carbonate can be used as reliable palaeoenvironmental indicator in zone 1 where the amount of ostracod remains was not sufficient to perform stable isotope analysis of shells (Figs. 5 and 8).

Stable isotope analyses of bulk samples were carried out using a Finnigan MAT 252 mass spectrometer (Thermo Fisher Scientific Co.) in the State Key Laboratory of the Lanzhou Institute of Geology, Chinese Academy of Sciences. For the analysis of the stable isotope data of the carbonate ($\delta^{18}O_{car}$ and $\delta^{13}C_{car}$), macroscopic remains of aquatic plants and mollusks were first removed from the samples. Afterwards, the samples were dried, powdered, and then placed into the vacuum system and heated for 1 h at approximately 300 °C. The samples were then reacted with 100% phosphoric acid in an 85–90 °C hot water bath for approximately 1 h. The produced CO_2 was trapped in a cold finger with liquid nitrogen. Then, the cold finger sample was moved to another cold finger trap by soaking in an approximately −75 °C alcohol-liquid-nitrogen bath to collect pure CO_2 before isotope ratios were measured using the Finnigan MAT 252 mass spectrometer. The results are reported in per mil relative to V-PDB by assigning a $\delta^{13}C$ value of +1.95‰ and a $\delta^{18}O$ value of −2.2‰ to the standard reference NBS 19. Reproducibility was checked systematically by replicate analysis of a laboratory standard every ten measurements and is better than ±0.2‰ (1σ).

3.3. Ostracod analysis

Samples of 1–2 cm thickness were taken from core C2 at intervals of 2–5.5 cm for ostracod analysis. The samples were freeze-dried and weighed before sieving. Dry samples with average weights of 5–10 g were disaggregated by 3% H_2O_2 for 48–72 h and washed with tap water through 100 μm and 250 μm meshes. The sieve residues were washed to plastic containers with 96% ethanol and dried in air. A minimum number of 300 ostracod shells were randomly picked from the samples. If sieve residues contained <300 ostracod shells, all ostracod shells were picked for identification. All shells of adult ostracods from 274 samples were picked from dried residues using a fine paint brush and a needle under an Olympus binocular microscope for quantitative statistics. A maximum of 485 shells were obtained from a sample of originally ~4 g dry weight. The shells were identified to genus and species levels based on publications by Meisch (2000), Van der Meeren et al. (2009) and Mischke and Zhang (2011). A SEM (Zeiss Supra 40 VP Scanning Electron Microscope at Freie Universität Berlin, Germany) was used to determine the marginal ripples on the posteroventral inner lamella of left *Ilyocypris* shells; while the other species were identified under the binocular. *Ilyocypris* cf. *bradyi* and *Tonnacypris* cf. *estonica* (Fig. 4) were identified with reservation because of lacking confirmation by soft-part analysis. Absolute abundances of ostracods were calculated and used for establishing five zones based on visual inspection (Fig. 6).

The ostracod-based transfer function for specific conductivity (SC) of Tibetan Plateau lakes was applied to the ostracod percentage data from core C2 (Mischke et al., 2007). This transfer function is based on ostracod percentage abundances of surface-sediment samples from 100 lakes including Lake Heihai and accompanying SC readings. Reconstructed SC values were calculated based on ostracod percentage data for each investigated sample horizon using the software C2 (Juggins, 2003). Conversion of SC values to salinity data was done by applying a conversion factor of 0.725 (Hölting, 1992).

Samples for stable isotope analyses of ostracod shells were selected from the picked shell materials. Stable oxygen and carbon isotope data were measured for adult shells of either *Leucocythere* sp. or *Limnocythere inopinata* due to the lack of one species recorded throughout the entire core. Two to nine adult shells of *Leucocythere* sp. and six to eight shells of *Limnocythere inopinata* were used per sample, with the weight ranging from 0.03 to 0.8 mg. The samples were reacted with 100% H_3PO_4 at 70 °C in an automated carbonate preparation device (KIEL IV) coupled with a Finnigan MAT 253 IRMS at the GeoForschungsZentrum in Potsdam, Germany. Stable isotope data are expressed in the delta notation relative to V-PDB (Peedee Belemnite) calibrated with NBS-19. The analytical precision is better than ±0.06‰ (1σ) for oxygen and ±0.04‰ for carbon isotopes. The resulting data were corrected to account for species-specific differences in $\delta^{13}C_{ost}$ and $\delta^{18}O_{ost}$ values as a result of vital effects in comparison to equilibrium precipitates (von Grafenstein et al., 1999) and different microhabitat preferences of *Leucocythere* sp. and *Limnocythere inopinata* (Mischke et al., 2010b; von Grafenstein et al., 1999; Decrouy, 2013). The vital effects of *Leucocythere* sp. for $\delta^{18}O_{ost}$ and $\delta^{13}C_{ost}$ values are −1.57‰ and 1.08‰, respectively. The vital effects of *Limnocythere inopinata* for $\delta^{18}O_{ost}$ and $\delta^{13}C_{ost}$ values are 1.2‰ and −1 to −3‰, respectively. Here, we used −2‰ as the vital effect of *Limnocythere inopinata* with respect to $\delta^{13}C_{ost}$ values. The number of ostracod shells was not sufficient to apply carbon and oxygen isotope analysis for zone 1.

4. Results

4.1. Bulk sediment analyses

Total organic carbon (TOC) shows strong fluctuations in the lower part of zone 1: the TOC content shows a rising trend in a range from 0.3 to 1.9% at the base of zone 1 from 667 to 610 cm, whilst it deceases between 610 and 572 cm. Afterwards, the TOC content increases to the top of zone 2 where TOC values vary from 1.8 to 4.8% with the median of 2.7% in the core. The TOC contents decline from zone 3 to the lower part of zone 5. The value increases at the upper part of zone 5 (Fig. 5).

The carbonate contents range from 8.0 to 75.0% with a median of 14.0% in zone 1. The value is low in the lower middle part of zone 1. The carbonate content increases to the highest values of 75.0% near the top

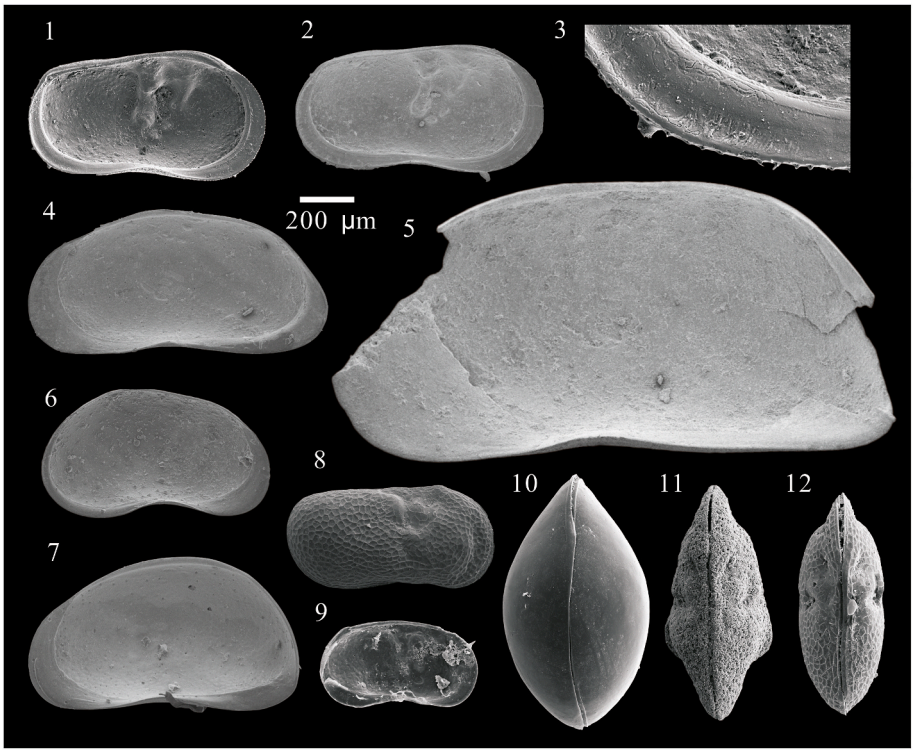

Fig. 4. Ostracod shells from Lake Heihai. 1–3, *Ilyocypris* cf. *bradyi* Sars, 2 and 3, left shell (L), internal view (i); 3, marginal ripplets of *Ilyocypris* cf. *bradyi*, enlargement of posteroventral area of specimen of 1.4, *Eucypris afghanistanensis* Hartmann, right shell (R), i. 5, *Tonnacypris* cf. *estonica* Järvekülg, R, i. 6, *Neglecandona neglecta* Sars, L, i. 7, *Candona candida* O. F. Müller, R, i. 8, *Leucocythere* sp., R, external shell (e). 9, *Limnocythere inopinata* Baird, L, i. 10, *Eucypris mareotica* Fischer, carapace in dorsal view. 11. *Leucocythere dorsotuberosa* Huang, carapace in dorsal view. 12, *Leucocythere* sp. carapace in dorsal view.

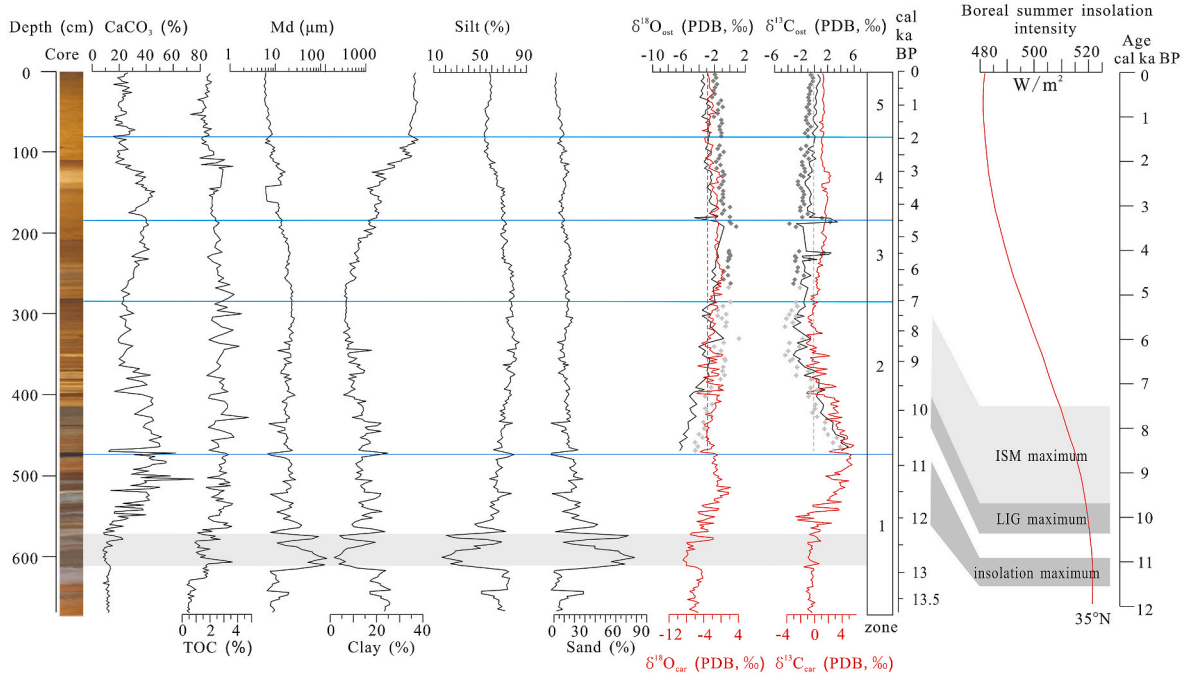

Fig. 5. Contents of $CaCO_3$ and total organic carbon (TOC), granulometric data, $\delta^{18}O_{ost}$ and $\delta^{13}C_{ost}$ data of ostracod calcite, $\delta^{18}O_{car}$ and $\delta^{13}C_{car}$ data of bulk sediments, and boreal summer insolation intensities (summer solstice) at 35°N (Laskar et al., 2004). Md represents median grain size. Two ostracod species were used for the stable isotope data of shells: *Limnocythere inopinata* (light grey crosses in the lower half), and *Leucocythere* sp. (dark grey rhombs). The black lines represent $\delta^{18}O_{ost}$ and $\delta^{13}C_{ost}$ values corrected for the species-specific differences between shells of *Limnocythere inopinata* and *Leucocythere* sp. Dashed lines represent the arithmetical mean. Zonation according to ostracod abundance data. ISM and LIG stand for Indian Summer Monsoon and Latitudinal Insolation Gradient, respectively. The time scale of boreal summer insolation intensities is equidistant.

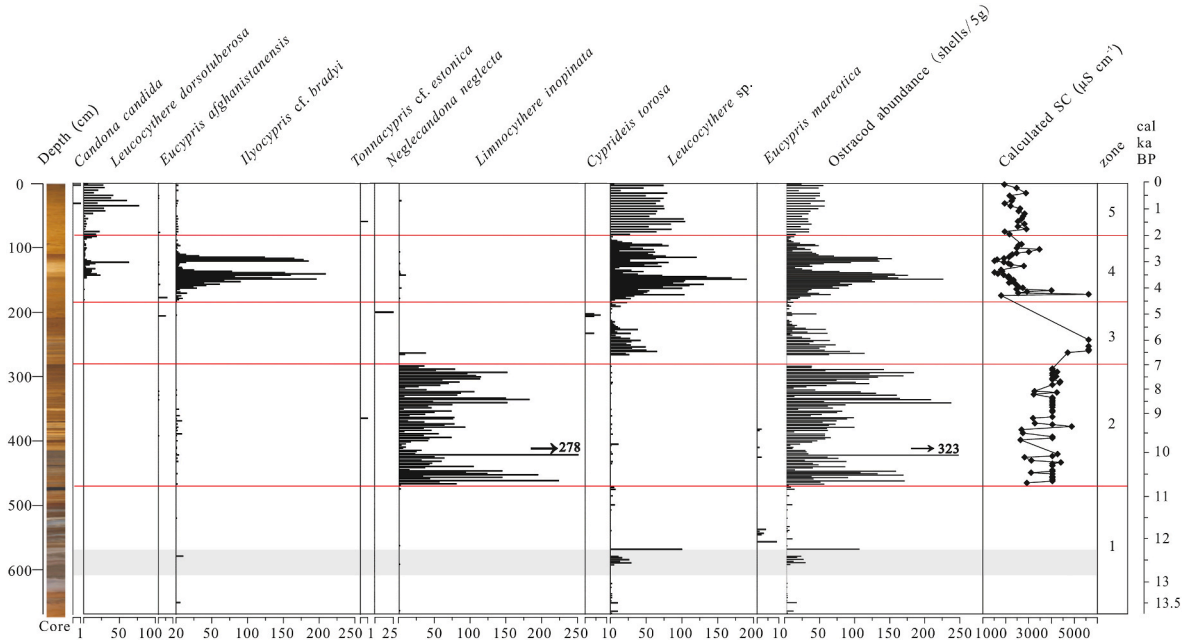

Fig. 6. Absolute ostracod abundances (shells per 5g of sediment) and reconstructed specific conductivities (SC) from Lake Heihai. SC was calculated based on the transfer function of Mischke et al. (2007). Species are arranged according to their SC optima with lowest optimum at left. Optima are based on the 100 lakes data set of Mischke et al. (2007) and additional data from lakes Heihai, Kusai, Haiding Nuur and Yanhu at the northern margin of the Tibetan Plateau, calculated as abundance-weighted SC averages of species occurrences (Zhang et al., 2013). Zonation according to ostracod abundance data.

of zone 1. In zone 2, the carbonate content shows a decline trend and varies from 12.4 to 61.9% with 30.2% as median. The content slightly increases to a median of 34.9% in zone 3, and decreases to medians of 29.7 and 22.5% in zones 4 and 5, respectively (Fig. 5).

The median grain sizes vary from 6.5 to 137.2 μm in zone 1. The value of 137.2 μm as the maximum recorded at the depth between 610 and 572 cm, where clay and silt portions reach the lowest values, respectively, change from 1.7% to 19.5% and from 17.0% to 68.6%; meanwhile, the content of sand reaches the highest values in the core, ranging from 11.9% to 81.3%. The median grain sizes are between 5.7

and 27.2 μm in zones 2 to 5, where the contents of clay, silt and sand vary from 5.7 to 37.9%, 53.4–83.8%, and 0.2–26.3%, respectively (Fig. 5).

The $\delta^{18}O_{car}$ values range from −8.8 to −1.9‰ (median −4.5‰) in zone 1 and from −7.8 to +2.2‰ in the zones above. The $\delta^{13}C_{car}$ values include the minimum of −2.7‰ in zone 1 and the maximum of +5.7‰ in zone 2 (Fig. 5).

The X-ray analysis of the lake sediment shows that the sediment is mainly composed of quartz, feldspar, calcite and dolomite (Fig. 7). Image analysis with a SEM revealed that authigenic carbonate grains are abundant in the lake sediment (Fig. 7).

4.2. Ostracod analyses

The ostracod shells found in the studied samples of core C2 belong to eight genera including ten species. *Leucocythere* sp. (previously identified as *Leucocythere mirabilis* by Mischke et al. (2007) and *Leucocytherella sinensis* by Mischke et al. (2008), *Eucypris mareotica* (Fischer, 1855, better known by its junior synonym *Eucypris inflata* Sars, 1930), *Ilyocypris* cf. *bradyi* Sars, 1890 and *Limnocythere inopinata* (Baird, 1843) are sporadically recorded in zone 1. Single shells of *Tonnacypris* cf. *estonica* (Järvekülg, 1960) are recorded at the depth of 359 cm in zone 2 and 59 cm in zone 5, respectively. *Limnocythere inopinata* is abundant in zone 2 whereas *Leucocythere* sp. is dominant from zone 3 to zone 5. *Neglecandona neglecta* (Sars, 1887) and *Cyprideis torosa* (Jones, 1850) only occur in zone 3. *Eucypris afghanistanensis* Hartmann, 1964 has high abundances in zone 4. *Leucocythere dorsotuberosa* Huang, 1982 is recorded in zone 4 and zone 5. Single shells of *Candona candida* (O.F. Müller, 1776) occurred at 31 and 3 cm in zone 5. The ostracod species composition shows a shift at 472 cm core depth (*ca.* 10.8 cal ka BP) with a significantly increased diversity in the upper part (Fig. 6).

Calculated SC values based on the relative ostracod abundances and the applied transfer function are mainly in a range from *ca.* 1500 μS cm^{-1} (salinity: *ca.* 1.1‰) to 4900 μS cm^{-1} (*ca.* 3.5‰). Maximum values of 5616 μS cm^{-1} (*ca.* 4.1‰) were determined for species assemblage data from 264 to 243 cm (*ca.* 6.5 to 6.0 cal ka BP; Fig. 6).

The $\delta^{13}C_{ost}$ values for *Leucocythere* sp. in the lower (587-567 cm) and the upper (261-3 cm) part of the core range from −3.78 to +2.41‰ with a median of −0.34‰. The $\delta^{18}O_{ost}$ values vary from −6.74 to +1.61‰ with a median of −2.65‰. The $\delta^{13}C_{ost}$ values for *Limnocythere inopinata* in the middle of the core (467-265 cm) are in the range of −4.45 to +3.92‰ with a median of −0.99‰; whereas their $\delta^{18}O_{ost}$ values vary between −4.52 and + 1.19‰ with a median of −3.21‰ (Fig. 5).

5. Discussion

5.1. The late glacial and Holocene evolution of Lake Heihai

5.1.1. Zone 1 (670-472 cm; before ca. 10.8 cal ka BP)

The TOC content, grain size and $\delta^{18}O_{car}$ values increase at the base of the zone (*ca.* 670-610 cm; *ca.* 13.7–12.9 cal ka BP; Fig. 5). Shells of *Leucocythere* sp., *Ilyocypris* cf. *bradyi* and *Limnocythere inopinata* occur sporadically (Fig. 6). According to sub-recent records of *Leucocythere* sp. from the Tibetan Plateau and adjacent areas (Mischke et al., 2007, 2008, 2010a, 2010b, 2010c; Zhang et al., 2013b, 2015), the taxon has a broad SC-tolerance range. *Leucocythere* sp. is well-adapted to harsh biotopes. It is a typical cold climate representative of Tibetan Plateau lakes (Mischke et al., 2008). The high specific conductivity optimum and broad tolerance range of *Leucocythere* sp. reflect its common habitats, often affected by rapid hydrochemical fluctuations (Mischke et al., 2007). Relatively abundant shells of *Leucocythere* sp. in water bodies of the Kunlun Mountain region were especially recorded in surface sediments from shallow depths between 0.2 and 1.5 m and unstable seasonal pond sites with an SC exceeding 2.8 mS cm^{-1} (Zhang et al., 2013b). The fine-grained sediments of zone 1 show that Lake Heihai already existed at the core location. The sporadic occurrences of ostracod shells indicate a low lake level and unstable hydrochemical conditions. Increasing TOC contents probably result from climate warming in the region. We assume that the increased evaporation driven by the temperature increase possibly resulted in the fluctuation of the hydrochemical conditions of the lake (Zhang et al., 2022).

Later on, decreasing TOC contents between 610 and 572 cm (*ca.* 12.9–12.3 cal ka BP) probably indicate lower lake productivity and colder conditions (Fig. 5). *Leucocythere* sp., as a salt-tolerant and typical cold climate species, probably indicates a more saline lake environment. An even lower lake level during a drought period is indicated by the dominating sand fraction in this part of the core, which accounts for 56.2% on average of the carbonate-free sediment. The reduction of vegetation in the catchment area under cold and dry climate conditions, the lowered soil water conservation capacity, the decline of the lake level and resulting shorter distance between the core location and the lake shore, as well as the enhanced hydrodynamic conditions at shallower water depth probably contributed to the significant increase in the load of coarse detrital particles which entered the lake (Liu et al., 2003; Wu and Shen, 2010). The carbonate content decreases to the lowest value at the depth of 590 cm (*ca.* 12.6 cal ka BP; Fig. 5). The $\delta^{18}O_{car}$ values drop from the previous period and reach lowest values in the core (−6.9‰ on average), and increase significantly later on. This increase probably results from stronger evaporation effects. The core site was possibly close to the lake shore or even above from time to time during the period from *ca.* 12.9–12.3 cal ka BP. Lake Heihai shrank and turned into a saline lake with minor inflowing streams which resulted in sand accumulation at the core location. This period corresponds to the global cold YD phase (Cheng et al., 2020) which occurred during the Last Glacial Termination.

After *ca.* 12.3 cal ka BP, the significantly rising TOC and carbonate contents possibly suggest increased temperatures resulting from higher solar irradiance at the glacial-Holocene transition (Fig. 5). Shells of *Ilyocypris* cf. *bradyi*, *Limnocythere inopinata*, *Leucocythere* sp. and the saline water species *Eucypris mareotica* are recorded occasionally with low abundances (Fig. 6). Lake-level changes were probably accompanied by substantial hydrochemical and physical fluctuations. We may assume that the significant increase of $\delta^{18}O_{car}$, carbonate content and TOC values resulted from larger evaporation effects with an increasing residence time of the lake water during a steady lake-level rise whilst the more or less stable values since *ca.* 11.5 cal ka BP represent the adjustment to a newly developed higher lake level. Generally, the lake productivity increased as a result of rising water temperatures in zone 1 (Fig. 5).

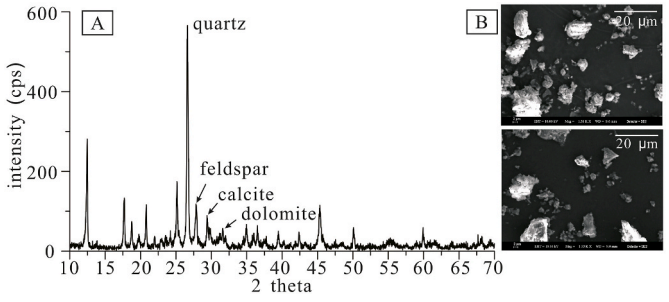

Fig. 7. A, X-ray diffraction result of Lake Heihai sediments; and B, scanning electron microscope images of sediments from Lake Heihai.

5.1.2. Zone 2 (472-283 cm; ca. 10.8-7.0 cal ka BP)

Continuously high TOC contents in zone 2 suggest relatively high lake productivity and relatively warm conditions. The carbonate content shows a decreasing trend. The sand content decreases mostly apart from the uppermost section of zone 2, whilst the silt content shows the opposite trend (Fig. 5). These changes probably indicate a high lake level and wet conditions. Ostracod shells become abundant and

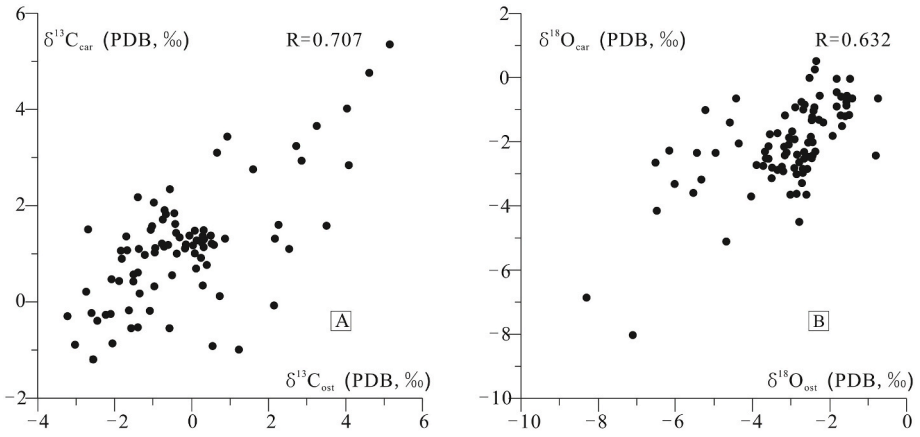

Fig. 8. A, $\delta^{13}C_{ost}$ versus $\delta^{13}C_{car}$ values; and B, $\delta^{18}O_{ost}$ *versus* $\delta^{18}O_{car}$ values.

constantly present in the zone. The euryhaline species *Limnocythere inopinata* dominates, accompanied by low abundances of *Eucypris afghanistanensis*, *Ilyocypris* cf. *bradyi*, *Eucypris mareotica* and *Leucocythere* sp. A single shell of *Tonnacypris* cf. *estonica* is recorded at 359 cm depth (Fig. 6). *Limnocythere inopinata* is one of the most widespread species in water bodies of the Tibetan Plateau (Mischke et al., 2002, 2003a, 2003b, 2007; Li et al., 2010). Although it has broad tolerances to important environmental factors such as water temperature, habitat type, water depth and salinity (Meisch, 2000), it is regarded as a summer and a polythermophilic species (Yin and Geiger, 1996; von Grafenstein et al., 1999; Meisch, 2000). It thrived best at 20 °C in laboratory culturing experiments recorded by Yin et al. (1999). Its dominance supports our assumption of relatively warm conditions between *ca*. 10.8–7.0 cal ka BP. Transfer-function inferred SC values range from 2648 to 4405 μS cm^{-1}, which represents an estimated salinity range from 1.9 to 3.2‰. Thus, Lake Heihai was probably an oligohaline lake during the formation of zone 2.

In zone 2, the $\delta^{18}O_{ost}$ and $\delta^{13}C_{ost}$ values are lower than the $\delta^{18}O_{car}$ and $\delta^{13}C_{car}$ values. We assume that the shells of the polythermophilic and bottom-dwelling species *L. inopinata* were mostly formed in summer at warmer water temperatures (Pérez et al., 2013) in contrast to inorganic carbonate which formed not only in summer but also during the rest of the year when water temperatures were colder.

The $\delta^{18}O_{car}$ values fluctuate rapidly in the middle of zone 2 reflecting strong salinity variations due to the changing ratio of evaporation and inflowing water (Fig. 5). A high lake level is inferred during this period in the early-middle Holocene. The relatively high insolation, on one hand, probably led to rising temperatures and an increased land-sea thermal contrast which strengthened the monsoon and caused more precipitation in the catchment, whilst, on the other hand, the temperature increase also enhanced the melting of snow and ice in the upper catchment which caused higher meltwater runoff (Fig. 5). The lower $\delta^{18}O_{ost}$ and $\delta^{18}O_{car}$ values in the lower part of zone 2 probably reflect the increasing summer monsoon precipitation and runoff resulting from higher contributions of melt water from ice, snow and frozen ground in the catchment. The clay fraction is higher in the lower part of zone 2 probably indicating the higher contribution of glacial rock flour from melting glaciers in the catchment.

The lake level was highest at *ca*. 10.8–7.0 cal ka BP with warmer and wetter conditions due to a strengthened summer monsoon.

5.1.3. Zone 3 (283-185 cm; ca. 7.0-4.5 cal ka BP)

The increased carbonate content and the decreased TOC content in zone 3 indicate cold conditions. The clay-sized clastic fraction increases (Fig. 5), probably resulting from advancing glaciers in the catchment and increased meltwater contribution from the lower parts of mountain areas to the lake.

Ostracod shells were not recorded at the base of zone 3 from *ca*. 7.0 to 6.6 cal ka BP., which possibly indicates prevailing unfavorable conditions. *Leucocythere* sp. occurs later on with relatively high abundances accompanied by a few shells of *L. inopinata*. The abundance of *Leucocythere* sp. decreases to the upper part of the zone, culminating in the replacement of *Leucocythere* sp. by shells of the brackish-water species *Cyprideis torosa* (recorded as the smooth-shelled form *C. torosa* cf. *littoralis*), and shells of *Neglecandona neglecta* between 211 and 196 cm core depth (*ca*. 5.2 to 4.8 cal ka BP; Fig. 6). *Cyprideis torosa* is widely recorded in brackish coastal waters throughout Europe, but it also occurs in continental water bodies of northern Africa, the Mediterranean region, North America and in arid Central Asia. Its salinity tolerance ranges from almost freshwater to hyperhaline habitats but it achieves largest abundances within 2–16.5‰, which is equivalent to 1450 to 12,000 μS cm^{-1} (Meisch, 2000). The species dominates in water bodies with SC values exceeding 5000 μS cm^{-1} and with high K and low Ca concentration in Israel (Mischke et al., 2010d). It was frequently recorded in surface and sediment-core samples from Bosten Lake in Xinjiang (Mischke and Schudack, 2001; Mischke and Wünnemann, 2006). However, it is not a common species on the Tibetan Plateau where it was only recorded with relatively low abundances from the middle Pleistocene Quan Ji section in the Qaidam Basin, and the Holocene sediments of Kuhai and Eastern Juyanze lakes in its northeastern part (Mischke et al., 2003a, 2003b, 2006, 2010c). *Neglecandona neglecta* was recorded frequently in Ulungur and Bosten lakes in Xinjiang Province and also in lakes of the Tibetan Plateau (identified as *Candona neglecta*, Mischke et al., 2002, 2007; Mischke and Wünnemann, 2006; Mischke and Zhang, 2011). A SC optimum of 1300 μS cm^{-1} was determined from six water bodies in Tibetan Plateau (Mischke et al., 2007).

Transfer-function based SC values range from 4705 to 5616 μS cm^{-1}, equal to a salinity from 3.4 to 4.1‰, 4.0‰ on average, which represents a rise compared to zone 2 (Fig. 6). The inferred higher salinity is supported by the monospecific occurrence of *Leucocythere* sp. in most samples of zone 3 because the species has relatively high conductivity optima of 7700 and 11145 μS cm^{-1}, reported by Mischke et al. (2007) and Zhang et al. (2013b), respectively. The $\delta^{18}O_{ost}$ values increase and are above average probably reflecting the evaporative concentration of lake water and relatively arid conditions compared to zone 2. The $\delta^{18}O_{car}$ values increase in the lower third of the zone with values ranging from −2.8 to +0.5‰, and they remain stable afterwards and higher than those of zone 2. The $\delta^{13}C_{car}$ and $\delta^{13}C_{ost}$ values are lower than those of zone 2, which probably indicates that the isotopic fractionation between lake-water CO_3^{2-} and atmospheric CO_2 is weaker in zone 3 due to decreased temperatures (Leng and Marshall, 2004; Myrbo and Shapley, 2006).

A decline in lake level and increase in lake-water salinity as a result of prevailing relatively cold and dry conditions is inferred for the period

from *ca.* 7.0–4.5 cal ka BP.

5.1.4. Zone 4 (185-80 cm; ca. 4.5-2.0 cal ka BP)

The TOC and carbonate contents, the sand fraction and $\delta^{13}C_{ost}$ values decrease from the base of zone 4 to *ca.* 175 cm core depth (*ca.* 4.5–4.3 cal ka BP; Fig. 5) suggesting that conditions were colder and the productivity was lower (von Grafenstein et al., 1999; Mischke et al., 2008; Li and Liu, 2014). The cold-climate representative *Leucocythere* sp. clearly dominates, accompanied by *Ilyocypris* cf. *bradyi* from *ca.* 4.3–3.5 cal ka BP and *ca.* 3.0–2.5 cal ka BP. *Ilyocypris bradyi* is a Holarctic species which was recorded as an abundant species in running water habitats, such as springs, streams and other slowly flowing waters (Mezquita et al., 1999; Meisch, 2000; Mischke et al., 2005; Mischke and Zhang, 2011). Shells of *I.* cf. *bradyi* were also more frequently recorded from running water habitats in the Qilian Mountains (Mischke et al., 2003b). Thus, the occurrence of *I.* cf. *bradyi* in the Lake Heihai record probably represents a mixture of shells which originated from inflowing streams and littoral lake waters. In addition, a few shells of *Eucypris afghanistanensis* are recorded at 175 cm depth (Fig. 6).

The carbonate content increases steadily from 175 to 145 cm (*ca.* 4.3–3.5 cal ka BP; Fig. 5) accompanied by slight increases of the $\delta^{13}C_{car}$ values and the sand fraction, possibly as response to higher productivity in the warmer waters of a shallower lake and the influx of detrital sediments from inflowing streams. *Leucocythere* sp. is frequently recorded in this part of zone 4, with highest abundances before *ca.* 3.5 cal ka BP. The abundance of *Ilyocypris* cf. *bradyi* increases significantly too. The higher numbers of *I.* cf. *bradyi* from *ca.* 4.3 to 3.5 cal ka BP indicate that the core location in Lake Heihai was influenced by nearby inflows.

From 145 cm to the top of the zone at 80 cm (*ca.* 3.5–2.0 cal ka BP; Fig. 5), the TOC and carbonate contents and the $\delta^{13}C_{car}$ values decrease, whilst the clay fraction and the $\delta^{13}C_{ost}$ values increase, indicating lower productivity due to colder conditions and a relatively higher influx of glacially-derived clastic sediment from advancing glaciers. The total ostracod abundance dropped between 145 and 125 cm (*ca.* 3.5–3.0 cal ka BP; Fig. 6). Afterwards, the ostracod assemblage is mostly dominated by *Leucocythere* sp. apart from the period from *ca.* 3.0 to 2.8 cal ka BP when *I.* cf. *bradyi* reached high numbers again, probably as a result of inflows near the core location. In addition, *Leucocythere dorsotuberosa* occurs consistently in this upper part of zone 4 and reaches a higher number at 125 cm (*ca.* 3.0 cal ka BP), whilst *Eucypris afghanistanensis* and *Limnocythere inopinata* were only recorded in a few samples with low abundances (Fig. 6). *Leucocythere dorsotuberosa* has been only recorded from the Tibetan Plateau and adjacent mountain ranges and it is probably restricted to this high-altitude region (Mischke et al., 2007; Frenzel et al., 2010; Zhang et al., 2013b). Shells of *L. dorsotuberosa* occur at twelve surface-sample locations in Lake Heihai with relatively low SC in a range from 0.6 to 1.8 mS cm^{-1} (equal to salinity ranging from 0.4 to 1.3‰). It typically reaches higher abundances at larger depth (>26 m) in Lake Donggi Cona although it was also reported from shallower locations (0.6–2.0 m; Mischke et al., 2010a). According to Akita et al. (2016), *L. dorsotuberosa* tolerates fresh to oligohaline waters with salinity up to 10‰, and it is characterized as cold stenothermal.

The higher $\delta^{18}O_{car}$ values and the low ostracod numbers from *ca.* 3.5–3.0 cal ka BP probably indicate that cold, unfavorable conditions prevailed (Figs. 5 and 6). Slightly lower $\delta^{18}O_{car}$ values accompanied by an increasing fraction of clay-sized particles after *ca.* 3.0 cal ka BP either suggest that the net-water input increased or/and evaporation effects weakened, or that the meltwater contribution increased. Considering the decreasing TOC and $\delta^{18}O_{car}$ values, the increasing clay-sized clastic fraction and the ostracod-assemblage data after *ca.* 3.5 cal ka BP together, we suggest that the contribution of meltwater from advancing glaciers under colder conditions was higher and that evaporation effects were reduced. The decrease in lake-water recharge and the decline of the lake level under cold conditions were assumed.

According to the results of the transfer-function application, the estimated SC fluctuated in a range from 1512 to 5616 μS cm^{-1}, 2392 μS cm^{-1} on average (equal to a salinity ranging from 1.1 to 4.1‰, 1.7‰ on average; Fig. 6), which is lower than those inferred for zone 3. The maximum estimate of 5616 μS cm^{-1} results from a single sample at 172 cm core depth near the base of the zone (*ca.* 4.2 cal ka BP), where a monospecific ostracod assemblage of *Leucocythere* sp. was recorded.

The $\delta^{18}O_{ost}$ values in zone 4 are generally comparable to those of the $\delta^{18}O_{car}$ values (Fig. 5). The similarity suggests that the water column of Lake Heihai was well mixed and that the lake was probably shallow (Mischke et al., 2008). Colder temperatures probably led to lower precipitation in the catchment and to a relatively increased accumulation of snow and ice, so that runoff to the lake was decreased, resulting in a lower lake level during the formation of zone 4. However, the inference of colder temperatures during the formation of zone 4 is not supported by significantly higher $\delta^{18}O_{ost}$ and $\delta^{18}O_{car}$ values in comparison to those of previous zones. The expected temperature-controlled increase in $\delta^{18}O_{ost}$ and $\delta^{18}O_{car}$ values was apparently counterbalanced by lowered $\delta^{18}O$ values of incoming precipitation in the catchment and by reduced evaporation effects on the lake waters under colder conditions. We assume that the lake level continuously dropped from zone 3 to zone 4, and that the core site was possibly relatively close to nearby inflows and the lake shore during most of the time.

5.1.5. Zone 5: (80-0 cm; ca 2.0-0 cal ka BP)

The TOC decreases from the base of the zone to *ca.* 50 cm core depth (*ca.* 2.0–1.2 cal ka BP; Fig. 5). The carbonate content increases first and decreases afterwards. The clay fraction increases in the same part of zone 5 whilst the sand fraction shows the opposite trend. The $\delta^{13}C_{car}$ and $\delta^{18}O_{car}$ values and the silt fraction remain more or less stable between the base of zone 5 and *ca.* 50 cm core depth. *Leucocythere* sp. dominates, accompanied by *Leucocythere dorsotuberosa* and *Ilyocypris* cf. *bradyi*. A single shell of *Tonnacypris* cf. *estonica* is recorded at 59 cm depth (Fig. 6). Colder climate conditions and advancing glaciers are inferred for the period from *ca.* 2.0 to 1.2 cal ka BP.

Above 50 cm depth (after *ca.* 1.2 cal ka BP), the TOC content increases steadily accompanied by a slight increase of the $\delta^{13}C_{ost}$ values. The clay and sand fractions first decrease and they remain more or less constant above whilst the silt fraction increases first and shows stable values near the top of the core. The abundance of the freshwater-indicating species *Leucocythere dorsotuberosa* is higher although *Leucocythere* sp. still dominates. A few shells of *Candona candida* are recorded at 31 cm and 3 cm, respectively (Fig. 6). The slightly higher TOC contents and lowered $\delta^{18}O_{car}$ and $\delta^{18}O_{ost}$ values above 50 cm probably indicate warmer conditions and a higher lake level as result of higher runoff entering the lake.

Transfer-function inferred SC estimates are slightly higher between *ca.* 2.0 to 1.2 cal ka BP (from 1958 to 2903 μS cm^{-1}, 2545 μS cm^{-1} on average; Fig. 6) than those after *ca.* 1.2 cal ka BP (from 1944 to 2882 μS cm^{-1}, 2385 μS cm^{-1} on average). The water level of Lake Heihai was lower between *ca.* 2.0 to 1.2 cal ka BP, accompanied by a higher salinity of lake water. Afterwards, the lake level rose and salinity decreased. The lake was mainly supplied by runoff from glacial meltwater (Ramisch et al., 2016).

5.2. Comparison with other records from adjacent areas of the Tibetan Plateau

Lake Heihai was probably a closed lake until about 10.8 cal ka BP, with cold and dry conditions during the period from *ca.* 12.9–12.3 cal ka BP and higher temperatures before and afterwards. Although the chronology of the Lake Heihai record from this section requires improvements, the inferred phase of cold and dry conditions during *ca.* 12.9–12.3 cal ka BP is in agreement with a number of palaeoclimate records from the northern hemisphere including records from the Tibetan Plateau (Shen et al., 2005; Walker et al., 2008, 2012; Opitz et al., 2012; Ramisch et al., 2018; Cheng et al., 2020). The onset of the Greenland Stadial 1 (i.e., the YD in the North Atlantic and northern

Europe), and its termination and the beginning of the Holocene are defined as *ca.* 12.9 and 11.7 cal ka BP, respectively, based on speleothem and ice-core oxygen-isotope data and other proxy records (Walker et al., 2008, 2012; Cheng et al., 2020). The cold phase recorded at Lake Heihai between *ca.* 12.9 and 12.3 cal ka BP is well in accordance with the YD period. Evidence for similar climate deterioration was recorded between 12.5 and 11.7 cal ka BP at Lake Naleng (Kramer et al., 2010). Comparable colder and drier conditions were also inferred as a slightly later period from other records from the Tibetan Plateau: during 12.2–10.9 cal ka BP in the Guliya ice core (Thompson et al., 1997; Yao, 1999), and during 11.8–11.2 cal ka BP from Hongyuan peat bog (Hong et al., 2003; Fig. 9). They were also detected at Sumxi Co and Longmu Co lakes between 10.5-9.9 ^{14}C ka BP (uncalibrated; Fontes et al., 1993), at Seling Co Lake between 10.8-10.0 ^{14}C ka BP (Gu et al., 1993), at Qinghai Lake between 11.3 and 10.8 cal ka BP (Shen et al., 2005), and at Lake Ximencuo culminating at ~10.6 cal ka BP (Zhang and Mischke, 2009). In contrast, an earlier cold and dry period was inferred from Lake Donggi Cona between 13.4 and 11.9 cal ka BP (Mischke et al., 2010b). The coincidence of the cold period recorded at Lake Heihai and the Greenland Stadial 1 suggests that the cold-dry YD period in the North Atlantic region probably influenced the Tibetan Plateau through a strengthened westerly circulation and the enhanced transport of cold and dry westerly air masses to Central Asia during summer. However, the significant differences in the determined timing of its onset and termination probably result from: 1) regional differences in response to global rapid climate change, 2) the different sensitivity of catchment systems and proxies to climate and environmental changes, and 3) insufficient chronological precision of the records partly reflecting the diversity of materials used for dating.

Warmer and wetter conditions with a highest lake level are inferred for Lake Heihai in the early-middle Holocene from *ca.* 10.8–7.0 cal ka BP. This result is well in accordance with warmest conditions inferred from Lake Bangong Co between 9.6-6.3 ^{14}C ka BP (calibrated age *ca.* 10.9–7.6 cal ka BP) and Lake Ximencuo from 10.4-6.0 ^{14}C ka BP (*ca.* 10.4–5.0 cal ka BP; Gasse et al., 1996; Zhang and Mischke, 2009; Herzschuh et al., 2014). There are also climate records from the Tibetan Plateau which indicate a significantly earlier establishment of warm and wet conditions: 12.8–7.1 cal ka BP at Lake Kuhai, 10.0–4.2 ^{14}C ka BP (*ca.* 11.6–5.8 cal ka BP) at Lake Seling Co, 11.5–7.2 ^{36}Cl ka BP at the Guliya ice cap, 9.9–6.0 ^{14}C ka BP (*ca.* 11.5–7.6 cal ka BP) at Sumxi Co-Longmu Co lakes, 11.5–6.0 cal ka BP at the Hongyuan peat sequence, and 11.4–6.3 cal ka BP at Lake Genggahai (Fontes et al., 1993; Gu et al., 1993; Gasse et al., 1996; Thompson, 2000; Hong et al., 2003; Zhang and Mischke, 2009; Mischke et al., 2010c; Qiang et al., 2017). A wet climate and stronger summer monsoon between 10.0 and 4.8 cal ka BP were suggested based on high A/C ratios and pollen concentrations from Dunde ice core (Liu et al., 1998). A significant and abrupt temperature increase at *ca.* 10.4 cal ka BP and highest precipitation during the first half of the Holocene (10.4–5.0 cal ka BP) were reconstructed for Lake Ximencuo at the eastern margin of the Tibetan Plateau based on pollen data (Herzschuh et al., 2014). Warmer conditions during the first half of the Holocene were also recorded at lakes Qinghai, Hurleg, Hala and Donggi Cona (with the periods of 10.8–4.5 cal ka BP, 11.1–4.8 cal ka BP, 11.5–7.5 cal ka BP and 11.9–6.8 cal ka BP, respectively; Shen et al., 2005; Mischke et al., 2010b; Yan and Wünnemann, 2014; Ma et al., 2021; Fig. 9). According to Zhang et al. (2021), inflow of glacial meltwater to Lake Heihai increased significantly after 11 cal ka BP and reached a maximum *ca.* 9 cal ka BP. Afterwards, meltwater inflow

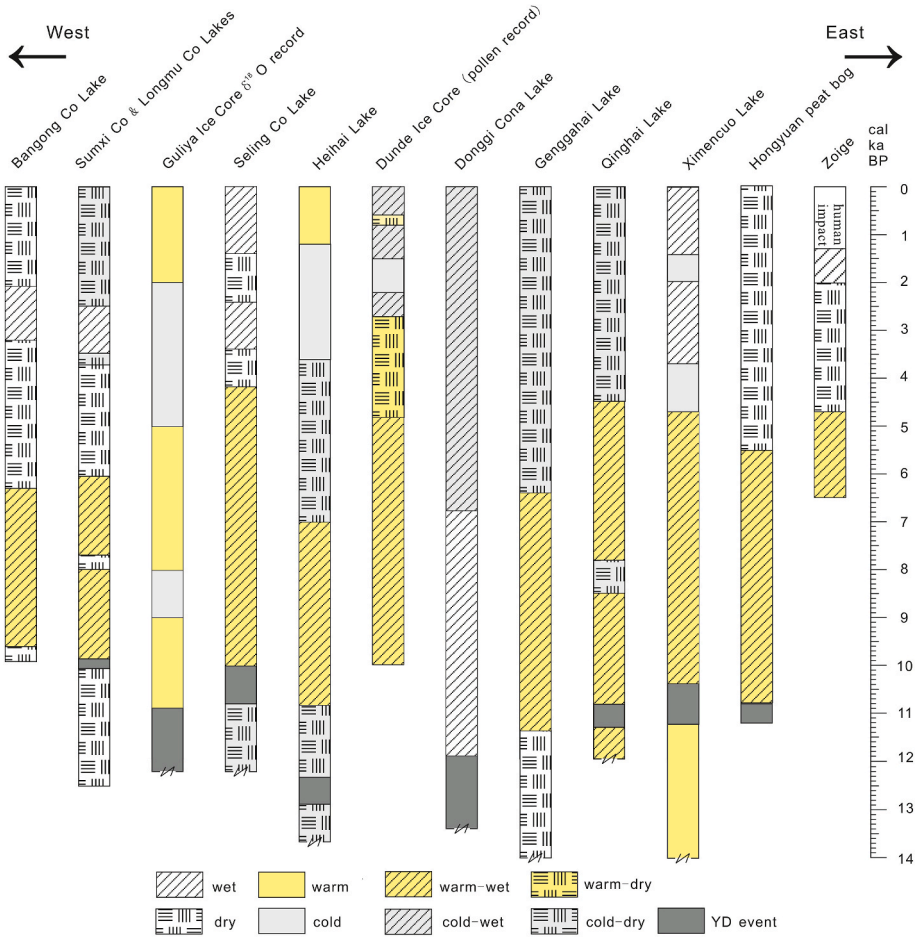

Fig. 9. Comparison of selected palaeoclimatic records for the Tibetan Plateau. Sites are arranged from west to east. References are provided in the caption of Fig. 1.

remained high until *ca.* 5.5 cal ka BP (Zhang et al., 2021). They also suggested that permafrost thawing in the catchment area and thermokarst processes in the lake basin played an important role for the water depth changes of Lake Heihai. However, the contribution of thawing permafrost to the water budget of the lake is controlled by various factors such as the specific climate conditions including seasonality changes, the rate and depth of permafrost thawing, and the local lithological and hydrological conditions (Jin et al., 2007, 2019; Zhao et al., 2019; Zhu et al., 2019). We argue that higher temperatures in the early-middle Holocene caused higher monsoonal precipitation in the catchment area and enhanced glacial meltwater discharge to the lake which both contributed to the reconstructed lake-level rise (Stauch et al., 2017). Lake Heihai is currently at the edge of the summer monsoon transition zone. The summer monsoon penetrated probably further to the northwest during the early-middle Holocene when insolation was significantly higher than today (Shen et al., 2005; Mischke et al., 2010b; Fig. 5). In general, the summer monsoon reached the northern, eastern and southern parts of the Tibetan Plateau during the early to middle Holocene although some spatio-temporal asynchronism occurred probably as a result of (1) the complex interplay of the East Asian and Indian summer monsoons, and the westerlies, (2) locally different effects of the temperature increase on the precipitation/evaporation ratio, and (3) different hydrological response times of individual, partly glaciated catchment areas. In addition, discrepancies between chronologies probably evolve from dating uncertainties such as unknown or poorly constrained lake-reservoir effects on radiocarbon dating.

Cold and dry conditions prevailed from *ca.* 7.0 to 4.5 cal ka BP, which is consistent with numerous records from the region. According to pollen records from the northwestern and northeastern parts of the Tibetan Plateau, cold and dry conditions culminated *ca.* 7.5–6.0 cal ka BP (Kong and Du, 1990; Sun et al., 1993; van Campo and Gasse, 1993). Dry climate was suggested based on diatom and pollen records from Lake Sumxi between 5.5 and 4.3 ^{14}C ka BP (*ca.* 6.3–5.1 cal ka BP; van Campo and Gasse, 1993). Schlütz and Lehmkuhl (2009) inferred a cooling phase since 5.9 cal ka BP from their Nianbaoyeze peat record. In the central Tibetan Plateau, cool-dry conditions were inferred from Lake Cuoe between 5.8 and 4.0 cal ka BP, and decreasing precipitation since 7.5 ka from Ahung Co (Morrill et al., 2006; Wu et al., 2006). In the Guliya ice core, a cooling event was recorded around 5.0 ^{36}Cl ka BP (Yao et al., 1997). Herzschuh et al. (2014) reconstructed a temperature decrease of about 3 °C at 5.0 cal ka BP based on their pollen data from Lake Ximencuo. Decreasing strength of the summer monsoon and the establishment of arid conditions after 5.5 cal ka BP was recorded from the Hongyuan-peat record (Hong et al., 2003). A weakened summer monsoon was recorded after *ca.* 5.0 cal ka BP in the western and after *ca.* 4.0 cal ka BP in the central parts of the Tibetan Plateau too (Shen and Tang, 1996). Therefore, significant mid-Holocene climate deterioration was widely recorded from the Tibetan Plateau region. Widespread drier conditions in the middle Holocene resulted from a weakening influence of the summer monsoon.

The middle Holocene climate instability including several cold periods is also inferred from the deposits and landforms of glaciers and especially from related ice margins on the Tibetan Plateau. Although the Asian monsoon precipitation is regarded as a major driver of glaciation in the Himalaya, the northeastern Tibetan Plateau and the Karakoram Mountains of Pakistan (Finkel et al., 2003; Owen et al., 2003; Gayer et al., 2006), Rupper et al. (2009) emphasized that glacial advances in the Himalaya during the early to mid-Holocene were influenced both by monsoon precipitation and temperature changes. Decreased summer temperatures resulted from an increase in cloudiness and an increase in evaporative cooling, and triggered the early-mid Holocene glacier advances (Rupper et al., 2009). Some studies suggest that glaciers on the Tibetan Plateau are apparently more sensitive to temperatures (Yao et al., 2012; Ou et al., 2014; Sati et al., 2014). For example, glacier advances were recorded at 7.5–4.5 ka BP (OSL ages) during an arid phase in the Dunagiri Valley in the western part of the Himalayas (Sati et al., 2014). Thus, Holocene local glacier fluctuations resulted from a combination of temperature and precipitation changes but cooling was probably the main factor of the Holocene glacier advances (Sati et al., 2014). A local and regional glacial stage of 6.9–4.3 ^{10}Be ka BP was inferred for the western Himalayan-Tibetan region. Denton and Karlén (1973) termed the period from 5.8 to 4.9 cal ka BP as the second new ice age with advances of all mountain glaciers in the northern and southern hemispheres. Dortch et al. (2013) summarized and recalculated ^{10}Be dates from 645 glacial landforms from the western Himalayan-Tibetan orogen, and they concluded that glacier advances after 21 ka were broadly associated with westerly winds. Thus, glacial dynamics in the western Himalayan-Tibetan orogen were probably related to cold events on the northern hemisphere and changes of global ice volumes. Most glacier advances since the last glaciation correspond to periods of low temperatures. Yi et al. (2008) suggested that the timing of Holocene glacier advances was synchronous with cooling periods identified in the δ^{18}O records of ice cores from the Tibetan Plateau. The low oxygen isotope values in the Guliya ice core record after 7 ^{36}Cl ka BP indicate the onset of cold conditions leading to a gradual decline in the Indian Summer Monsoon (Thompson et al., 1997). The middle Holocene glacier advances in the northwestern part of the Himalayan-Tibetan orogen were attributed to the reduced northern hemisphere insolation and southerly-shifted westerly belts (Saha et al., 2018; Fig. 9). Insolation-driven cooling probably increased the influence of the mid-latitude westerly circulation, and triggered glacier advances in the catchment of Lake Heihai between 7.0 and 4.5 cal ka BP (Yao et al., 2012; Stauch et al., 2017).

Lake Heihai was characterized by a lower water level under colder conditions during the late Holocene between *ca.* 4.5 and 2.0 cal ka BP. The influx of glacially derived clastic sediments increased significantly during this period, probably as a result of glacier advances and the enhanced glacial meltwater contribution in comparison to catchment precipitation in the region (Owen et al., 2006). Cold conditions in the late Holocene probably corresponded to a weakening of the Indian Summer Monsoon triggered by the gradual decrease of boreal summer insolation (Ramisch et al., 2016; Fig. 5). The climate deterioration during this period is consistent with records from elsewhere in the region. Evidence from most parts of the Tibetan Plateau suggests that the late Holocene climate was cold and dry (Shen et al., 2005; Mischke et al., 2008; Zhang and Mischke, 2009; Opitz et al., 2012; Xu et al., 2019). Abrupt climate events were reported by Morrill et al. (2003) for monsoon-influenced regions at approximately 4.5 cal ka BP. Dry climate was suggested based on pollen records from the Zoige Basin between 4.7 and 2.0 ^{14}C ka BP in the eastern Tibetan Plateau (*ca.* 5.4 to 2.7 cal ka BP, Zhao et al., 2011). The pollen record from the Dunde ice core from the northern Tibetan Plateau implied a cold period from 2.7 to 2.2 cal ka BP (Liu et al., 1998). Records from the northeastern and eastern parts of the Tibetan Plateau show that dry and cold conditions prevailed after 4.5 and 4.3 ka BP at Lake Qinghai and Lake Donggi Cona, respectively, between 4.3 and 2.0 cal ka BP at Lake Koucha and between 4.2 and 2.8 cal ka BP at Lake Ximencuo (Shen et al., 2005; Mischke et al., 2008; Zhang and Mischke, 2009; Opitz et al., 2012). Correspondingly, a low lake level was reconstructed from Lake Luanhaizi (Herzschuh et al., 2005). Dry and cold conditions and enhanced westerlies during 4.0–1.3 cal ka BP were suggested from Lake Buruo Co on the northern Tibetan Plateau (Xu et al., 2019).

Glacier advances were reported from the northeastern and eastern parts of the Tibetan Plateau after 4.5 cal ka BP (Ou et al., 2014; Xu et al., 2016; Qiang et al., 2017). Three late Holocene glacial advances in the Hailuogou catchment were simulated by a quantitative reconstruction (Xu et al., 2016). Regional glacial stages of 3.8, 3.1 and 2.5 cal ka BP were inferred from Lake Genggahai (Qiang et al., 2017). Approximately 2-km long glacier advances occurred in the Yingpu Valley during the Late Holocene (Ou et al., 2014). Cold conditions were also indicated by low δ^{18}O values between 4.0 and 2.7 cal ka BP and 3.8–2.4 cal ka BP in

the Puruogangri and the Guliya ice-core records from the central and northwestern Tibetan Plateau, respectively (Thompson et al., 1997, 2006).

The cold conditions in the Lake Heihai region from *ca.* 2.0 to 1.2 cal ka BP are consistent with inferences from a number of sites on the Tibetan Plateau. According to lake sediment records, cold conditions prevailed from 1.7 to 1.3 cal ka BP at Lake Ximencuo (Mischke and Zhang, 2010), 1.9–1.7 cal ka BP at Lake Buruo Co (Xu et al., 2019), 1.7–1.1 cal ka BP at Lake Kalakuli (Liu et al., 2014) and 1.7–1.5 cal ka BP at Lake Nam Co (Zhu et al., 2008). Cold periods were also recorded by peat deposits from the Nianbaoyeze Mountains and Hongyuan at 1.5 and 2.0 cal ka BP, respectively (Schlütz and Lehmkuhl, 2009; Zheng et al., 2011). Cold spells during this part of the late Holocene were also inferred from the deposits of glaciers, such as those in the Muztag Ata and Kongur Shan region, and from the Guliya and Dunde ice cores (Yao and Thompson, 1992; Thompson et al., 1997; Seong et al., 2009). The pollen records from Zoige Basin and Lake Zigetang implied a cold period at 2.4–1.3 cal ka BP and 1.4–1.1 cal ka BP, respectively (Herzschuh et al., 2006; Zhao et al., 2011).

Slightly warmer conditions afterwards inferred from our record have been reported from a wide region on the Tibetan Plateau too. A relatively warm and wet climate was recorded in the Zoige Basin from 1.3 to 0.5 cal ka BP according to the pollen record of Zhao et al. (2011). The onset of warmer conditions since the early 20th century was inferred from higher $\delta^{18}O$ values in the Guliya, Dunde, Dasuopu and Puruogangri ice cores (Thompson, 2000; Thompson et al., 2006). Our inference of a warm period after *ca.* 1.2 cal ka BP is in contrast to the cold and dry conditions recorded from 2.5 to 0 cal ka BP at Qinghai Lake (Shen et al., 2005). The conflicting inferences probably result from different sensibilities of regions at lower and higher altitudes to warming (Yao et al., 2012). According to observational data from the Tibetan Plateau, the warming rate increases with elevation and is highest between 4800 and 6200 m a.s.l. (Qin et al., 2009). Lake Heihai is located at higher altitude (~4400 m a.s.l.) than Qinghai Lake (~3200 m a.s.l.), and thus, Lake Heihai probably responds faster to changing climate conditions. Furthermore, the relatively small glaciers in the catchment of Lake Heihai responded probably rapidly to global warming (Yao et al., 2012). In 2014, small ice caps and valley glaciers still existed in the south of the lake (Stauch et al., 2017). Therefore, originally larger and probably additional glaciers retreated during the warming period, resulting in a higher meltwater contribution to Lake Heihai with the consequence of a rising lake level.

6. Conclusions

The sediment core from Lake Heihai represents a continuous late glacial and Holocene record of environmental changes in the catchment area and provides important information with respect to climate change, water resources and glacier fluctuations in the northern Tibetan Plateau. In addition, the evolution of the lake, especially with regard to salinity and lake-level changes was inferred from the multi-proxy record.

Lake Heihai remained a closed lake until about 10.8 cal ka BP, with cold and dry conditions during the period from *ca.* 12.9–12.3 cal ka BP and less cold temperatures before and afterwards. Warmer and wetter conditions with increased water level and lower salinity were recorded at Lake Heihai between *ca.* 10.8 and 7.0 cal ka BP in response to the strengthened summer monsoon. A widespread 8.2 cal ka BP cold event was not evidently recorded from the sediment of Lake Heihai. Cold and dry conditions prevailed from *ca.* 7.0 to 4.5 cal ka BP and resulted in a declined lake level and increased lake-water salinity. Glacier advances in the catchment of Lake Heihai during this period were probably triggered by the increased influence of the mid-latitude westerly circulation. Cold conditions, glacier advances and low lake levels prevailed until *ca.* 1.2 cal ka BP. Warmer conditions and a higher water level of Lake Heihai as result of higher runoff entering the lake were recorded after *ca.* 1.2 cal ka BP.

The late glacial and Holocene climate of the Tibetan Plateau and adjacent regions was characterised by spatial heterogeneity. Thus, more studies of palaeoclimate records are required to better understand the regional climate evolution. Derived climate inferences from the study region will surely benefit from more reliable chronological control and analyses of additional proxies such as pollen or biomarker data. Especially quantitative inferences of precipitation and temperature changes have great potential to improve our understanding of the local effects of environmental and climate change. Such better understanding is required to better assess hydrological conditions and water resources in climatically especially sensitive regions of the world.

Data availability

The original data of this study are available upon request from the corresponding author.

CRediT authorship contribution statement

Wanyi Zhang: Conceptualization, Material and data collection, Methodology, Analysis, Writing – original draft, Writing – review & editing, Visualization. **Steffen Mischke:** Conceptualization, Writing – original draft, Writing – review & editing, Writing – review & editing, Supervision. **Dominic Hosner:** Conceptualization, Writing – original draft, Writing – review & editing, Visualization. **Chengjun Zhang:** Conceptualization, Methodology, Analysis, Writing – original draft, Writing – review & editing, Supervision. **Birgit Plessen:** Methodology, Analysis. **Huwei Li:** Material and data collection. **Xiaojing Zhang:** Material and data collection.

Declaration of competing interest

The authors declare that they have no known competing financial interests or personal relationships that could have appeared to influence the work reported in this paper.

Acknowledgements

We appreciate Bernd Wünnemann (Southwest Jiaotong University, Chengdu; Freie Universität Berlin) who kindly provided the core samples. We thank Hao Chen, Lianfu Zhou for providing data, and Dada Yan and Yongzhan Zhang for help during fieldwork. Detailed and constructive comments on a first manuscript draft or later versions by David B. Madsen (University of Texas and Lanzhou University), Tomasz Goslar (Poznan Radiocarbon Laboratory, Adam Mickiewicz University), Christian Leipe (Max Planck Institute of Geoanthropology), Gregori Lockot, Pavel E. Tarasov (both Freie Universität Berlin) and three anonymous reviewers were greatly appreciated. We thank Sylvia Pinkerneil (Helmholtz-Centre Potsdam-GFZ German Research Centre for Geosciences) for help with measuring oxygen and carbon stable isotopes of ostracod shells.

The research was supported by The Second Tibetan Plateau Scientific Expedition and Research (STEP) program (2019QZKK0704), Fundamental Research Funds for the Central Universities, Lanzhou University (lzujbky-2019-46) and the National Natural Science Foundation of China (41571177).

References

Akita, L.G., Frenzel, P., Wang, J.B., Börner, N., Peng, P., 2016. Spatial distribution and ecology of the Recent Ostracoda from Tangra Yumco and adjacent waters on the southern Tibetan Plateau: a key to palaeoenvironmental reconstruction. Limnologica 59, 21–43.

An, F.Y., Lai, Z.P., Liu, X.J., Wang, Y.X., Chang, Q.F., Lu, B.L., Yang, X.Y., 2018a. Luminescence chronology and radiocarbon reservoir age determination of lacustrine sediments from the Heihai Lake, NE Qinghai-Tibetan Plateau and its paleoclimate implications. J. Earth Sci. 29, 695–706.

An, F.Y., Liu, X.J., Zhang, Q.X., Wang, Y.X., Chen, T.Y., Yu, L.P., Lu, B.L., Chang, Q.F., 2018b. Drainage geomorphic evolution in response to paleoclimatic changes since 12.8 ka in the eastern Kunlun Mountains, NE Qinghai-Tibetan Plateau. Geomorphology 319, 117–132.
Bao, S.D., 1999. Soil Chemical Analysis. Chinese Agriculture Press, Beijing, pp. 30–34 in Chinese.
Chang, Q., Lai, Z., An, F., Wang, H.L., Lei, Y.B., Han, F.Q., 2017. Chronology for terraces of the Nalinggele River in the north Qinghai-Tibet Plateau and implications for salt lake resource formation in the Qaidam Basin. Quat. Int. 430, 12–20.
Chen, F.H., Zhang, J.F., Liu, J.B., Cao, X.Y., Hou, J.Z., Zhu, L.P., Xu, X.K., Liu, X.J., Wang, M.D., Wu, D., Huang, L.X., Zeng, T., Zhang, S., Huang, W., Zhang, X., Yang, K., 2020. Climate change, vegetation history, and landscape responses on the Tibetan Plateau during the Holocene: a comprehensive review. Quat. Sci. Rev. 243, 106444.
Cheng, H., Zhang, H.W., Spötl, C., Baker, J., Sinha, A., Li, H.Y., Bartolomé, M., Moreno, A., Kathayat, G., Zhao, J.Y., Dong, X.Y., Li, Y.W., Ning, Y.F., Jia, X., Zong, B. Y., Brahim, Y.A., Pérez-Mejías, C., Cai, Y.J., Novello, V.F., Cruz, F.W., Severinghaus, J.P., An, Z.S., Edwards, R.L., 2020. Timing and structure of the Younger Dryas event and its underlying climate dynamics. Proc. Natl. Acad. Sci. USA 117, 23408–23417.
Cyr, H., Downing, J.A., 1988. The abundance of phytophilous invertebrates on different species of submerged macrophytes. Freshw. Biol. 1988, 365–374.
De Deckker, P., 1981. Ostracods of athalassic saline lakes. Hydrobiologia 81, 131–144.
De Deckker, P., Chivas, A.R., Shelley, J.M.G., Torgersen, T., 1988. Ostracod shell chemistry: a new palaeoenvironmental indicator applied to a regressive/transgressive record from the Gulf of Carpentaria, Australia. Palaeogeogr. Palaeoclimatol. Palaeoecol. 66, 231–241.
Decrouy, L., 2013. Biological and Environmental Controls on Isotopes in Ostracod Shells. In: Horne, D., Holmes, J., Rodriguez-Lazaro, J., Viehberg, F. (Eds.), Ostracoda as Proxies for Quaternary Climate Change. Elsevier, Oxford, pp. 165–181.
Denton, G.H., Karlén, W., 1973. Holocene climatic variations - their pattern and possible cause. Quat. Res. 3, 155–174.
Dortch, J.M., Owen, L., Caffee, M.W., 2013. Timing and climatic drivers for glaciation across semi-arid western Himalayan-Tibetan orogen. Quat. Sci. Rev. 78, 188–208.
Finkel, R.C., Owen, L.A., Barnard, P.L., Caffee, M.W., 2003. Beryllium-10 dating of Mount Everest moraines indicates a strong monsoonal influence and glacial synchroneity throughout the Himalaya. Geology 31, 561–564.
Fontes, J.C., Mélières, F., Gibert, E., Liu, Q., Gasse, F., 1993. Stable isotope and radiocarbon balances of two Tibetan lakes (Sumxi Co, Longmu Co) from 13,000 BP. Quat. Sci. Rev. 12, 875–887.
Frenzel, P., Wrozyna, C., Xie, M.P., Zhu, L.P., Schwalb, A., 2010. Palaeo-water depth estimation for a 600-year record from Nam Co (Tibet) using an ostracod-based transfer function. Quat. Int. 218, 157–165.
Gasse, F., Fontes, J.C., Van Campo, E., Wei, K., 1996. Holocene environmental changes in Bangong Co basin (Western Tibet) Part 4: discussion and conclusions. Palaeogeogr. Palaeoclimatol. Palaeoecol. 120, 79–92.
Gayer, E., Lavé, J., Pik, R., France-Lanord, C., 2006. Monsoonal forcing of Holocene glacier fluctuations in Ganesh Himal (Central Nepal) constrained by cosmogenic ^{3}He exposure ages of garnets. Earth Planet Sci. Lett. 252, 275–288.
Gu, Z.Y., Liu, J.G., Yuan, B.Y., Liu, T.S., Liu, R.M., Liu, Y., Zhang, G.Z., 1993. The changes in monsoon influence in the Qinghai-Tibetan Plateau during the past 12,000 years. Geochemical evidence from the lake sediments. Chin. Sci. Bull. 38, 61–64 in Chinese.
Herzschuh, U., Borkowski, J., Schewe, J., Mischke, S., Tian, F., 2014. Moisture-advection feedback supports strong early-to-mid Holocene monsoon climate on the eastern Tibetan Plateau as inferred from a pollen-based reconstruction. Palaeogeogr. Palaeoclimatol. Palaeoecol. 402, 44–54.
Herzschuh, U., Winter, K., Wünnemann, B., Li, S., 2006. A general cooling trend on the central Tibetan Plateau throughout the Holocene recorded by the Lake Zigetang pollen spectra. Quat. Int. 154–155, 113–121.
Herzschuh, U., Zhang, C.J., Mischke, S., Herzschuh, R., Mohammadi, F., Mingram, B., Kürschner, H., Riedel, F., 2005. A late Quaternary lake record from the Qilian Mountains (NW China): evolution of the primary production and the water depth reconstructed from macrofossil, pollen, biomarker, and isotope data. Global and Planet. Change 46, 361–379.
Hirokazu, O., 2003. Japan Sea ostracod assemblages in surface sediments: their distribution and relationship to water mass properties. Paleontol. Res. 7, 257–274.
Holmes, J.A., Fothergill, P.A., Street-Perrott, F.A., Perrott, R.A., 1998. A high resolution Holocene ostracod record from the Sahel zone of Northeastern Nigeria. J. Paleolimnol. 20, 369–380.
Holmes, J.A., Zhang, J.W., Chen, F.F., Qiang, M.R., 2007. Paleoclimatic implications of an 850-year oxygen-isotope record from the northern Tibetan Plateau. Geophys. Res. Lett. 34, L23403.
Hölting, B., 1992. Hydrogeologie. Einführung in die allgemeine und angewandte Hydrogeologie. Enke, Stuttgart, p. 425 in German.
Hong, Y.T., Hong, B., Lin, Q.H., Zhu, Y.X., Shibata, Y., Hirota, M., Uchida, M., Leng, X.T., Jiang, H.B., Xua, H., Wang, H., Yi, L., 2003. Correlation between Indian ocean summer monsoon and north atlantic climate during the Holocene. Earth Planet Sci. Lett. 211, 371–380.
Jin, H.J., Chang, X.L., Wang, S.L., 2007. Evolution of permafrost on the Qinghai-Xizang (Tibet) Plateau since the end of the late Pleistocene. J. Geophys. Res. 112, F02S09.
Jin, H.J., Jin, X.Y., He, R.X., Luo, D.L., Chang, X.L., Wang, S.L., Marchenko, S., Yang, S. Z., Yi, C.L., Li, S.J., Harris, S.A., 2019. Evolution of permafrost in China during the last 20 ka. Sci. China Earth Sci. 62, 1207–1223.
Juggins, S. User Guide C2, Software for Ecological and Palaeoecological Data Analysis and Visualisation, User Guide Version 1.3. Department of Geography, Newcastle (2003).
Kidd, W.S.F., Yusheng, P., Chengfa, C., Coward, M.P., Dewey, J.F., Gansser, A., Molnar, P., Shackleton, R.M., Yiyin, S., 1988. Geological mapping of the 1985 Chinese-British Tibetan (Xizang-Qinghai) plateau geotraverse route. Philosophical Transactions of the Royal Society of London. Series A 327, 287.
Kong, S.C., Du, N.Q., 1990. Vegetational and climate changes in the last 11000 years in Qinghai Lake-numerical analysis based on Palynology in core QH85-14C. Mar. Geol. Quat. Geol. 10, 79–90 in Chinese with English abstract.
Kramer, A., Herzschuh, U., Mischke, S., Zhang, C., 2010. Late glacial vegetation and climate oscillations on the southeastern Tibetan Plateau inferred from the Lake Naleng pollen profile. Quat. Res. 73, 324–335.
Leng, M.J., Marshall, J.D., 2004. Palaeoclimate interpretation of stable isotope data from lake sediment archives. Quat. Sci. Rev. 23, 811–831.
Li, H., Van Der Woerd, J., Tapponnier, P., Klinger, Y., Qi, X., Yang, J., Zhu, Y., 2005. Slip rate on the Kunlun fault at Hongshui Gou, and recurrence time of great events comparable to 14/11/2001, Mw~7.9 Kokoxili earthquake. Earth Planet Sci. Lett. 237, 285–299.
Li, X., 1989. The Holocene sediments and movement rate of active faults in Dali Basin and migration of ancient bank of Erhai Lake. Quaternaria Sinica 8, 65–73 in Chinese.
Li, X.Z., Liu, W.G., 2014. Water salinity and productivity recorded by ostracod assemblages and their carbon isotopes since the early Holocene at Lake Qinghai on the northeastern Qinghai-Tibet Plateau, China. Palaeogeogr. Palaeoclimatol. Palaeoecol. 407, 25–33.
Li, X.Z., Liu, W.G., Xu, L.M., 2012. Stable oxygen isotope of ostracods in recent sediments of Lake Gahai in the Qaidam Basin, northwest China: The implications for paleoclimatic reconstruction. Global and Planet. Change 94–95, 13–19.
Li, X.Z., Liu, W.G., Zhang, L., Sun, Z.C., 2010. Distribution of recent ostracod species in the Lake Qinghai area in northwestern China and its ecological significance. Ecol. Indicat. 10, 880–890.
Lister, G.S., Kelts, K., Chen, K.Z., Jun, Q.Y., Niessen, F., 1991. Lake Qinghai, China: closed basin lake levels and the oxygen isotope record for ostracoda since the latest Pleistocene. Palaeogeogr. Palaeoclimatol. Palaeoecol. 84, 141–162.
Liu, K.B., Yao, Z.J., Thompson, L.G., 1998. A pollen record of Holocene climatic changes from the Dunde ice cap, Qinghai-Tibetan Plateau. Geology 26, 135–138.
Liu, S., Kruse, S., Scherler, D., Ree, R.H., Zimmermann, H.H., Stoof-Leichsenring, K.R., Epp, L.S., Mischke, S., Herzschuh, U., 2021. Sedimentary ancient DNA reveals a threat of warming-induced alpine habitat loss to Tibetan Plateau plant diversity. Nat. Commun. 12, 2995.
Liu, X.Q., Herzschuh, U., Wang, Y.B., Kuhn, G., Yu, Z.T., 2014. Glacier fluctuations of Muztagh Ata and temperature changes during the late Holocene in westernmost Tibetan Plateau, based on glaciolacustrine sediment records. Geophys. Res. Lett. 41, 6265–6273.
Liu, X.Q., Shen, J., Wang, S.M., Wang, Y.B., Liu, W.G., 2007. Southwest monsoon changes indicated by oxygen isotope of ostracode shells from sediments in Qinghai Lake since the late Glacial. Chin. Sci. Bull. 52, 539–544.
Liu, X.Q., Wang, S.M., Shen, J., 2003. The grainsize of the core QH-2000 in Qinghai Lake and its implication for paleoclimate and paleoenvironment. J. Lake Sci. 1 (5), 112–117 in Chinese with English abstract.
Lockot, G., Ramisch, A., Wünnemann, B., Hartmann, K., Haberzettl, T., Chen, H., Diekmann, B., 2015. A process- and provenance-based attempt to unravel inconsistent radiocarbon chronologies in lake sediments: an example from Lake Heihai, North Tibetan Plateau (China). Radiocarbon 57, 1003–1019.
Ma, X.Y., Wei, Z.F., Wang, Y.L., Wang, G., Zhang, T., He, W., Yu, X.L., Ma, H., Zhang, P. Y., Li, S.K., Wei, J.Y., Fan, Q.H., 2021. Reconstruction of climate changes based $\delta^{18}O_{carb}$ on the Northeastern Tibetan Plateau: a 16.1-cal kyr BP record from Hurleg Lake. Front. Earth Sci. 9, 745972.
Maussion, F., Scherer, D., Mölg, T., Collier, E., Curio, J., Finkelnburg, J., 2014. Precipitation seasonality and variability over the Tibetan Plateau as resolved by the High Asia reanalysis. J. Clim. 27, 1910–1927.
Meisch, C., 2000. Freshwater Ostracoda of western and central Europe. In: Süsswasserfauna von Mitteleuropa, 8/3. Spektrum Akademischer Verlag, Heidelberg.
Mezquita, F., Tapla, G., Roca, J.R., 1999. Ostracoda from springs on the eastern Iberian Peninsula: ecology, biogeography and palaeolimnological implications. Palaeogeogr. Palaeoclimatol. Palaeoecol. 148, 65–85.
Mischke, S., Aichner, B., Diekmann, B., Herzschuh, U., Plessen, B., Wünnemann, B., Zhang, C.J., 2010b. Ostracods and stable isotopes of a late glacial and Holocene lake record from the NE Tibetan Plateau. Chem. Geol. 276, 95–103.
Mischke, S., Almogi-Labin, A., Ortal, R., Schwab, M.J., Boomer, I., 2010d. Quantitative reconstruction of lake conductivity in the Quaternary of the Near East (Israel) using ostracods. J. Paleolimnol. 43, 667–688.
Mischke, S., Bößneck, U., Diekmann, B., Herzschuh, U., Jin, H.J., Kramer, A., Wünnemann, B., Zhang, C.J., 2010a. Quantitative relationship between water-depth and sub-fossil ostracod assemblages in Lake Donggi Cona, Qinghai Province, China. J. Paleolimnol. 43, 589–608.
Mischke, S., Demske, D., Schudack, M.E., 2003a. Hydrologic and climatic implications of a multidisciplinary study of the mid to late Holocene Lake Eastern Juyanze. Chin. Sci. Bull. 48, 1411–1417.
Mischke, S., Fuchs, D., Riedel, F., Schudack, M.E., 2002. Mid to late Holocene palaeoenvironment of lake eastern Juyanze (northwestern China) based on ostracods and stable isotopes. Geobios 35, 99–110.
Mischke, S., Herzschuh, U., Kürschner, H., Fuchs, D., Chen, F.H., Meng, F., Sun, Z.C., 2003b. Sub-recent Ostracoda from Qilian Mountains (NW China) and their ecological significance. Limnologica 33, 280–292.
Mischke, S., Herzschuh, U., Massmann, G., Zhang, C., 2007. An ostracod-conductivity transfer function for Tibetan lakes. J. Paleolimnol. 38, 509–524.

Mischke, S., Herzschuh, U., Sun, Z.C., Qiao, Z.Z., Sun, N.D., Zander, A.M., 2006. Middle Pleistocene Ostracoda from a large freshwater lake in the presently dry Qaidam Basin (NW China). J. Micropalaeontol. 25, 57–64.
Mischke, S., Herzschuh, U., Zhang, C.J., Bloemendal, J., Riede, F., 2005. A Late Quaternary lake record from the Qilian Mountains (NW China): lake level and salinity changes inferred from sediment properties and ostracod assemblages. Global Planet. Change 46, 337–359.
Mischke, S., Kramer, M., Zhang, C., Shang, H., Herzschuh, U., Erzinger, J., 2008. Reduced early Holocene moisture availability in the Bayan Har Mountains, northeastern Tibetan Plateau, inferred from a multi-proxy lake record. Palaeogeogr. Palaeoclimatol. Palaeoecol. 264, 211–212.
Mischke, S., Schudack, M.E., 2001. Sub-recent Ostracoda from Bosten Lake, NW China. J. Micropalaeontol. 20, 12.
Mischke, S., Wünnemann, B., 2006. The Holocene salinity history of Bosten Lake (Xinjiang, China) inferred from ostracod species assemblages and shell chemistry: possible palaeoclimatic implications. Quat. Int. 154–155, 100–112.
Mischke, S., Zhang, C.J., 2010. Holocene cold events on the Tibetan Plateau. Global Planet. Change 72, 155–163.
Mischke, S., Zhang, C.J., 2011. Ostracod distribution in Ulungur lake (Xinjiang, China) and a reassessed Holocene record. Ecol. Res. 26, 133–145.
Mischke, S., Zhang, C.J., Börner, A., Herzschuh, U., 2010c. Lateglacial and Holocene variation in aeolian sediment flux over the northeastern Tibetan Plateau recorded by laminated sediments of a saline meromictic lake. J. Quat. Sci. 25, 162–177.
Morrill, C., Overpeck, J.T., Cole, J.E., 2003. A synthesis of abrupt changes in the Asian summer monsoon since the last deglaciation. Holocene 13, 465–476.
Morrill, C., Overpeck, J.T., Cole, J.E., Liu, K.B., Shen, C.M., Tang, L.Y., 2006. Holocene variations in the Asian monsoon inferred from the geochemistry of lake sediments in central Tibet. Quat. Res. 65, 232–243.
Mourguiart, P., Carbonel, P., 1994. A quantitative method of palaeolake-level reconstruction using ostracod assemblages: an example from the Bolivian Altiplano. Hydrobiologia 288, 183–193.
Myrbo, A., Shapley, M.D., 2006. Seasonal water-column dynamics of dissolved inorganic carbon stable isotopic compositions ($\delta^{13}C_{DIC}$) in small hardwater lakes in Minnesota and Montana. Geochem. et Cosmochim. Acta 70, 2699–2714.
Opitz, S., Wünnemann, B., Aichner, B., Dietze, E., Hartmann, K., Herzschuh, U., Ijmker, J., Lehmkuhl, F., Li, S., Mischke, S., Plotzki, A., Stauch, G., Diekmann, B., 2012. Late glacial and Holocene development of lake Donggi Cona, north-eastern Tibetan plateau, inferred from sedimentological analysis. Palaeogeogr. Palaeoclimatol. Palaeoecol. 337–338, 159–176.
Ou, X.J., Lai, Z.P., Zhou, S.Z., Zeng, L.H., 2014. Timing of glacier fluctuations and trigger mechanisms in eastern Qinghai–Tibetan Plateau during the late Quaternary. Quat. Res. 81, 464–475.
Owen, L.A., Finkel, R.C., Ma, H., Barnard, P.L., 2006. Late Quaternary landscape evolution in the Kunlun Mountains and Qaidam Basin, Northern Tibet: a framework for examining the links between glaciation, lake level changes and alluvial fan formation. Quat. Int. 154–155, 73–86.
Owen, L.A., Finkel, R.C., Ma, H., Spencer, J.Q., Derbyshire, E., Barnard, P.L., Caffee, M. W., 2003. Timing and style of Late Quaternary glaciations in NE Tibet. Geol. Soc. Am. Bull. 15, 1356–1364.
Peng, J.L., 1997. Ostracod assemblages and environmental changes during 13000-4500 a B.P. in Peiku Co, Tibet. Acta Micropalaeontol. Sin. 14, 239–254 in Chinese with English abstract.
Peng, P., Zhu, L.P., Frenzel, P., Wrozyna, C., Ju, J.T., 2013. Water depth related ostracod distribution in Lake Pumoyum Co, southern Tibetan Plateau. Quat. Int. 313–314, 47–55.
Pérez, L., Lorenschat, J., Massaferro, J., Pailles, C., Sylvestre, F., Hollwedel, W., Brandorff, G.O., Brenner, M., Gerald, I., Lozano, M.D., Scharf, B., 2013. Bioindicators of climate and trophic state in lowland and highland aquatic ecosystems of the Northern Neotropics. Rev. Biol. Trop. 61, 603–644.
Qiang, M.R., Chen, F.H., Zhang, J.W., Zu, R.P., Jin, M., Zhou, A.F., Xiao, S., 2006. Grain size in sediments from Lake Sugan: a possible linkage to dust storm events at the northern margin of the Qinghai-Tibetan Plateau. Environ. Geol. 51, 1229–1238.
Qiang, M.R., Song, L., Jin, Y.X., Li, Y., Liu, L., Zhang, J.W., Zhao, Y., 2017. 16-ka oxygen-isotope record from Genggahai Lake on the northeastern Qinghai-Tibetan Plateau: hydroclimatic evolution and changes in atmospheric circulation. Quat. Sci. Rev. 162, 72–87.
Qin, J., Yang, K., Liang, S.L., Guo, X.F., 2009. The altitudinal dependence of recent rapid warming over the Tibetan Plateau. Clim. Change 97, 321–327.
Ramisch, A., Lockot, G., Haberzettl, T., Hartmann, K., Kuhn, G., Lehmkuhl, F., Schimpf, S., Schulte, P., Stauch, G., Wang, R., Wünnemann, B., Yan, D.D., Zhang, Y. Z., Diekmann, B., 2016. A persistent northern boundary of Indian summer monsoon precipitation over Central Asia during the Holocene. Sci. Rep. 6, 25791.
Ramisch, A., Tjallingii, R., Hartmann, K., Diekmann, B., Brauer, A., 2018. Echo of the younger Dryas in Holocene lake sediments on the Tibetan Plateau. Geophys. Res. Lett. 45, 11154–11163.
Rupper, S., Roe, G., Gillespie, A., 2009. Spatial patterns of Holocene glacier advance and retreat in Central Asia. Quat. Res. 72, 337–346.
Saha, S., Owen, L.A., Orr, E.N., Caffee, M.W., 2018. Timing and nature of Holocene glacier advances at the northwestern end of the Himalayan-Tibetan orogen. Quat. Sci. Rev. 187, 177–202.
Sati, S.P., Ali, S.N., Rana, N., Bhattacharya, F., 2014. Timing and extent of Holocene glaciations in the monsoon dominated Dunagiri vally (Bangni glacier), central Himalaya, India. J. Asian Earth Sci. 91, 125–136.
Schlütz, F., Lehmkuhl, F., 2009. Holocene climatic change and the nomadic Anthropocene in Eastern Tibet: palynological and geomorphological results from the Nianbaoyeze Mountains. Quat. Sci. Rev. 28, 1449–1471.
Seong, Y.B., Owen, L.A., Yi, C., Finkel, R.C., 2009. Quaternary glaciation of Muztag Ata and Kongur Shan: evidence for glacier response to rapid climate changes throughout the Late Glacial and Holocene in westernmost Tibet. Geol. Soc. Am. Bull. 121, 348–365.
Shen, C.M., Tang, L.Y., 1996. Pollen evidence of changing Holocene monsoon on Qinghai-Xizang Plateau. Acta Micropalaeontol. Sin. 13, 433–436 in Chinese with English abstract.
Shen, J., Liu, X.Q., Wang, S.M., Ryo, M., 2005. Palaeoclimatic changes in the Qinghai Lake area during the last 18,000 years. Quat. Int. 136, 131–140.
Stauch, G., Schulte, P., Ramisch, A., Hartmann, K., Hülle, D., Lockot, G., Diekmann, B., Nottebaum, V., Müller, C., Wünnemann, B., Yan, D.D., Lehmkuhl, F., 2017. Landscape and climate on the northern Tibetan Plateau during the late Quaternary. Geomorphology 286, 78–92.
Sun, A.Z., Feng, Z.D., 2022. Holocene moisture variations across the Tibetan Plateau: a synthesis of pollen records. Rev. Palaeobot. Palynol. 297, 104581.
Sun, X.J., Du, N.Q., Chen, Y.S., Gu, Z.Y., Liu, J.Q., Yuan, B.Y., 1993. Holocene palynological records in Lake Selincuo, Northern Xizang. Acta Bot. Sin. 35, 943–950 in Chinese with English abstract.
Tatzber, M., Stemmer, M., Spiegel, H., Katzlberger, C., Haberhauer, G., Gerzabek, M.N., 2007. An alternative method to measure carbonate in soils by FI-IR spectroscopy. Environ. Chem. Lett. 5, 9–12.
Thompson, L.G., 2000. Ice core evidence for climate change in the Tropics: implications for our future. Quat. Sci. Rev. 19, 19–35.
Thompson, L.G., Yao, T.D., Davis, M.E., Henderson, K.A., Mosley-Thompson, E., Lin, P. N., Beer, J., Synal, H.-A., Cole-Dai, J., Bolzan, J.F., 1997. Tropical climate instability: the last glacial cycle from a Qinghai-Tibetan Ice Core. Science 276, 1821–1825.
Thompson, L.G., Yao, T.D., Davis, M.E., Mosley-Thompson, E., Mashiotta, T.A., Lin, P.N., Mikhalenko, V.N., Zagorodnov, V.S., 2006. Holocene climate variability archived in the Puruogangri ice cap on the central Tibetan Plateau. Ann. Glaciol. 43, 61–69.
van Campo, E., Gasse, F., 1993. Pollen-and diatom-inferred climatic and hydrological changes in Sumxi Co Basin (Western Tibet) since 13,000 yr B.P. Quat. Res. 39, 300–313.
Van der Meeren, T., Khand, Y., Martens, K., 2009. On recent species of *Tonnacypris* Diebel and Pietrzeniuk, 1975 (Crustacea, Ostracoda), with new species descriptions from Mongolia. Zootaxa 2015, 1–41.
Van Der Woerd, J., Tapponnier, P., Ryerson, F.J., Meriaux, A.-S., Meyer, B., Gaudemer, Y., Finkel, R.C., Caffee, M.W., Gouguang, Z., Zhiqin, X., 2002. Uniform postglacial slip-rate along the central 600 km of the Kunlun Fault (Tibet), from ^{26}Al, ^{10}Be, and ^{14}C dating of riser offsets, and climatic origin of the regional morphology. Geophys. J. Int. 148, 356–388.
von Grafenstein, U., Erlernkeuser, H., Trimborn, P., 1999. Oxygen and carbon isotopes in modern fresh-water ostracod valves: assessing vital offsets and autecological effects of interest for palaeoclimate studies. Palaeogeogr. Palaeoclimatol. Palaeoecol. 148, 133–152.
Walker, M.J.C., Berkelhammer, M., Björck, S., Cwynar, L.C., Fisher, D.A., Long, A.J., Lowe, J.J., Newnham, R.M., Rasmussen, S.O., Weiss, H., 2012. Formal subdivision of the Holocene series/epoch: a discussion paper by a working group of INTIMATE (integration of icecore, marine and terrestrial records) and the subcommission on quaternary stratigraphy (international commission on stratigraphy). J. Quat. Sci. 27, 649–659.
Walker, M.J.C., Johnsen, S., Rasmussen, S.O., Steffensen, J.P., Popp, T., Gibbard, P., Hoek, W., Lowe, J., Björck, S., Cwynar, L.C., Hughen, K., Kershaw, P., Kromer, B., Litt, T., Lowe, D.J., Nakagawa, T., Newnham, R., Schwander, J., 2008. The global stratotype section and point (GSSP) for the base of the Holocene series/epoch (Quaternary system/period) in the NGRIP ice core. Episodes 31, 264–267.
Wang, S.M., Dou, H.S., 1998. The Record of Chinese Lakes. Science Press, Beijing, p. 491 in Chinese.
Wang, Y.B., Liu, X.Q., Han, L., Ni, Z.Y., Ma, X.Z., Wei, Y.R., Li, Z., 2021. Late Holocene climate variation on the northern Tibetan Plateau inferred from Lake Ayakum. Catena 207, 105599.
Wu, J., Shen, J., 2010. Paleoclimate evolution since 27.7 ka BP reflected by grain size variation of a sediment core from Lake Xingkai, northeastern Asia. J. Lake Sci. 22, 110–118.
World Climate. http://www.worldclimate.com/.
Wu, Y.H., Andreas, L., Jin, Z.D., Wang, S.M., Gerhard, H.S., Richard, W.B., Xia, W.L., 2006. Holocene climate development on the central Tibetan Plateau: a sedimentary record from Cuoe Lake. Palaeogeogr. Palaeoclimatol. Palaeoecol. 234, 328–340.
Xiao, J.L., Chang, Z.G., Si, B., Qin, X.G., Itoh, S., Lomtatidze, Z., 2008. Partitioning of the grainsize components of Dali Lake core sediments: evidence for lake-level changes during the Holocene. J. Paleolimnol. 40, 519–528.
Xiao, J.L., Fan, J.W., Zhai, D.Y., Wen, R.L., Qin, X.G., 2015. Testing the model for linking grain-size component to lake level status of modern clastic lakes. Quat. Int. 355, 34–43.
Xu, T., Zhu, L.P., Lv, X.M., Ma, Q.F., Wang, J.B., Ju, J.T., 2019. Mid- to late-Holocene paleoenvironmental changes and glacier fluctuations reconstructed from the sediments of proglacial lake Buruo Co, northern Tibetan Plateau. Palaeogeogr. Palaeoclimatol. Palaeoecol. 517, 74–85.
Xu, X.K., Muhammad, A.Q., Pan, B.L., 2016. Late-Holocene glacier advances and related climate conditions in the Hailuogou catchment, Gongga Shan, eastern Tibetan Plateau. Holocene 26, 1897–1903.
Yan, D.D., Wünnemann, B., 2014. Late Quaternary water depth changes in Hala Lake, northeastern Tibetan Plateau, derived from ostracod assemblages and sediment properties in multiple sediment records. Quat. Sci. Rev. 95, 95–114.
Yao, T.D., 1999. Abrupt climatic changes on the Tibetan Plateau during the Last Ice Age-Comparative study of the Guliya ice core with the Greenland GRIP ice core. Sci. China, Ser. A D 42, 358–368.

Yao, T.D., Thompson, L.G., 1992. Trends and features of climatic changes in the past 5000 years recorded by the Dunde ice core. Ann. Glaciol. 16, 21–24.
Yao, T.D., Thompson, L.G., Shi, Y.F., Qin, D.H., Jiao, K.Q., Yang, Z.H., Tian, L.D., Thompson, E.M., 1997. Climatic variation since the Last Interglacial recorded in the Guliya ice core. Sci. China (D) 40, 662–668.
Yao, T.D., Thompson, L.G., Yang, W., Yu, W.S., Gao, Y., Guo, X.J., Yang, X.X., Duan, K.Q., Zhao, H.B., Xu, B.Q., 2012. Different glacier status with atmospheric circulations in Tibetan Plateau and surroundings. Nat. Clim. Change 2, 663–667.
Yi, C.L., Chen, H.L., Yang, J.Q., Liu, B., Fu, P., Liu, K.X., Li, S.J., 2008. Review of Holocene glacial chronologies based on radiocarbon dating in Tibet and its surrounding mountains. J. Quat. Sci. 23, 533–543.
Yin, Y., Geiger, W., 1996. Thermal adaptation in *Limnocythere inopinata* clones - a comparison of life history traits at three different temperatures, 8-12 Juillet 1996. In: 3ème Congr. Européen des Ostracodologists. Paris-Bierville, p. 84. abstract.
Yin, Y., Geiger, W., Martens, K., 1999. Effects of genotype and environment on phenotypic variability in *Limnocythere inopinata* (Crustacea: Ostracoda). Hydrobiologia 400, 85–114.
Zhang, C.J., Fan, R., Li, J., Mischke, S., Dembele, B., Hu, X.L., 2013. Carbon and oxygen isotopic compositions: how lacustrine environmental factors respond in northwestern and northeastern China. Acta Geol. Sin. 87, 1344–1354.
Zhang, C.J., Mischke, S., 2009. A Lateglacial and Holocene lake record from the Nianbaoyeze Mountains and inferences of lake, glacier and climate evolution on the eastern Tibetan Plateau. Quat. Sci. Rev. 28, 1970–1983.
Zhang, C.J., Zhang, W.Y., Cheng, D.S., Yang, N., Hou, X.Y., Li, H.W., Zhang, X.J., Ayyamperumal, R., 2022. Hydrochemical characteristics and paleoclimate changes recorded from Sugan Lake on the northern boundary of Tibetan Plateau since mid-Holocene. Catena 217, 106527.
Zhang, W.Y., Mischke, S., Zhang, C.J., Gao, D., Fan, R., 2013. Ostracod distribution and habitat relationships in the Kunlun Mountains, northern Tibetan Plateau. Quat. Int. 313–314, 38–46.
Zhang, W.Y., Mischke, S., Zhang, C.J., Zhang, H.R., Wang, P., 2015. Sub-recent sexual populations of *Limnocythere inopinata* recorded for the first time from > 3500 m altitude on the Tibetan Plateau. Acta Geol. Sin. 89, 1041–1042.
Zhang, X.S., 2007. Vegetation Map of China and its Geographic Pattern - Illustration of Vegetation Map of People's Republic of China. Geology Publishing House, Beijing, 1 : 1,000,000.
Zhang, Y.Z., Wünnemann, B., Yan, D.D., Lockot, G., 2021. Late Quaternary persistent impacts of permafrost on lake hydrology and landscape evolution on the NE Tibetan Plateau. Quat. Sci. Rev. 274, 10728.
Zhao, L., Hu, G.J., Zou, D.F., Wu, X.D., Ma, L., Sun, Z., Yuan, L.M., Zhou, H.Y., Liu, S.B., 2019. Permafrost changes and its effects on hydrological processes on Qinghai-Tibet Plateau. Bull. Chin. Acad. Sci. 34, 1233–1246 in Chinese with English abstract.
Zhao, Y., Yu, Z.C., Zhao, W.W., 2011. Holocene vegetation and climate histories in the eastern Tibetan Plateau: controls by insolation-driven temperature or monsoon-derived precipitation changes? Quat. Sci. Rev. 30, 1173–1184.
Zheng, Y.H., Zhou, W.J., Meyers, P.A., 2011. Proxy value of n-alkan-2-ones in the Hongyuan peat sequence to reconstruct Holocene climate changes on the eastern margin of the Tibetan Plateau. Chem. Geol. 288, 97–104.
Zhu, D.G., Meng, X.G., Zhao, X.T., Shao, Z.G., Yang, C.B., Ma, Z.B., Wu, Z.H., Wang, J.P., 2004. Evolution and climate change of Nam Co of Tibet and an ancient large lake in the northern Tibetan Plateau since the late Pleistocene. Chin. Geol. 31, 269–277 in Chinese with English abstract.
Zhu, L.P., Chen, L., Li, B.Y., Li, Y.F., Xia, W.L., Li, J.G., 2002. Environmental changes reflected by the lake sediments of the South Hongshan Lake, northwest Tibet. Sci. China (Ser. D) 45, 430–439.
Zhu, L.P., Ju, J.T., Qiao, B.J., Yang, R.M., Liu, C., Han, B.P., 2019. Recent lake changes of the Asia Water Tower and their climate response: progress, problems and prospects. Chin. Sci. Bull. 64, 2796–2806 in Chinese with English abstract.
Zhu, L.P., Ju, J.T., Wang, Y., Xie, M.P., Wang, J.B., Peng, P., Zhen, X.L., Lin, X., 2010. Composition, spatial distribution, and environmental significance of water ions in Pumayum Co catchment, southern Tibet. J. Geogr. Sci. 20, 109–120.
Zhu, L.P., Wu, Y.H., Wang, J.B., Lin, X., Ju, J.T., Xie, M.P., Li, M.H., Mäusbacher, R., Schwalb, A., Daut, G., 2008. Environmental changes since 8.4 ka reflected in the lacustrine core sediments from Nam Co, central Tibetan Plateau, China. Holocene 18, 831–839.